Venus trap in the mouse embryo reveals distinct molecular dynamics underlying specification of first embryonic lineages

Jens-Erik Dietrich[1,†,‡], Laura Panavaite[1,†], Stefan Gunther[2], Sebastian Wennekamp[1], Anna C Groner[3,#], Anton Pigge[4], Stefanie Salvenmoser[1], Didier Trono[3], Lars Hufnagel[2] & Takashi Hiiragi[1,*]

Abstract

Mammalian development begins with the segregation of embryonic and extra-embryonic lineages in the blastocyst. Recent studies revealed cell-to-cell gene expression heterogeneity and dynamic cell rearrangements during mouse blastocyst formation. Thus, mechanistic understanding of lineage specification requires quantitative description of gene expression dynamics at a single-cell resolution in living embryos. However, only a few fluorescent gene expression reporter mice are available and quantitative live image analysis is limited so far. Here, we carried out a fluorescence gene-trap screen and established reporter mice expressing Venus specifically in the first lineages. Lineage tracking, quantitative gene expression and cell position analyses allowed us to build a comprehensive lineage map of mouse pre-implantation development. Our systematic analysis revealed that, contrary to the available models, the timing and mechanism of lineage specification may be distinct between the trophectoderm and the inner cell mass. While expression of our trophectoderm-specific lineage marker is upregulated in outside cells upon asymmetric divisions at 8- and 16-cell stages, the inside-specific upregulation of the inner-cell-mass marker only becomes evident at the 64-cell stage. This study thus provides a framework toward systems-level understanding of embryogenesis marked by high dynamicity and stochastic variability.

Introduction

Mammalian development is characterized by the pre-implantation stage during which the blastocyst forms with a single-layer epithelium, the trophectoderm (TE), surrounding a fluid-filled cavity and an eccentric inner cell mass (ICM). Upon implantation, TE will give rise to extra-embryonic tissues, whereas the epiblast cells within ICM will form the embryo proper. Two models have been proposed for the mechanism underlying the first lineage segregation between TE and ICM in the mouse embryo. The inside–outside model suggests that cell position in the morula regulates cell fate [1]; the inside cells with circumferential cell contacts contribute to the ICM, whereas cells facing the outside surface of the embryo form TE. The cell polarity model proposes that the apico-basal polarity of the blastomeres underlies cell fate differentiation [2]. Depending on the cleavage plane orientation relative to the apico-basal polarity, the 8- to 16- and 16- to 32-cell divisions generate either symmetric (two TE) or asymmetric (ICM and TE) descendants. Notably, in both models, the ICM vs. TE cell fate decision is binary and acquisition of molecular lineage-identity was considered to be regulated in a reciprocal manner [3]. Recent studies, however, revealed overlapping mosaic expression of the transcription factors that confer molecular identity to the first lineages [4–6]. In particular, the inside cells of the early blastocyst exhibit stochastic cell-to-cell variability in gene expression [7,8]. These data are incompatible with the above-mentioned models, and thus, the mechanism underlying the first lineage specification remains to be further investigated.

Recent developments in live imaging of the early mouse development revealed unprecedented dynamics during early mouse embryogenesis [9–13]. Live imaging analysis was enhanced by imaging transgenic embryos expressing fluorescence-labeled nuclei, which allowed tracking of all cells during pre-implantation development and generating lineage trees [14,15]. Given the dynamicity

1 Developmental Biology Unit, European Molecular Biology Laboratory (EMBL), Heidelberg, Germany
2 Cell Biology and Biophysics Unit, European Molecular Biology Laboratory (EMBL), Heidelberg, Germany
3 School of Life Sciences, Ecole Polytechnique Fédérale de Lausanne (EPFL), Lausanne, Switzerland
4 Max Planck Institute for Molecular Biomedicine, Muenster, Germany
 *Corresponding author. Tel: +49 6221 3878844; E-mail: hiiragi@embl.de
 †These authors contributed equally to this work
 ‡Present address: Department of Gynecologic Endocrinology and Fertility Disorders, Heidelberg University Women's Hospital, Heidelberg, Germany
 #Present address: Division of Molecular and Cellular Oncology, Department of Medical Oncology, Dana-Farber Cancer Institute and Department of Medicine, Brigham and Women's Hospital and Harvard Medical School, Boston, MA, USA

and stochastic molecular heterogeneity, mechanistic understanding of the first lineage specification requires quantitative description of the gene expression dynamics in living embryos during morphogenesis at single-cell resolution [16]. However, to date, only a limited number of fluorescence gene expression reporter mice suitable for live imaging are available [5,17–19], quantitative analysis of gene expression dynamics has begun only recently [19], and it has not been systematically integrated with cell lineage segregation pattern.

To analyze endogenous gene and protein expression dynamics, targeted knock-in of fluorescence-fusion reporters is often ideal [20]. However, this can result in transgenic embryos expressing low-level fluorescence signal, which is unsuitable for live imaging and subsequent image analysis. On the other hand, gene trap introduces random integration of a fluorescence reporter into the genome and the transgenic embryos suitable for live imaging can be selected by microscopic screenings. Gene-trap screenings have been carried out in various model organisms [21–23] and have generated valuable resources for live imaging embryonic development. However, mouse gene traps have thus far been primarily designed for genetic loss-of-function studies and expression analysis in fixed (e.g., by LacZ reporter), but not in live, tissues [24,25]. This may partly be because in mouse, embryonic development can be observed through live imaging only for a limited period of time. However, recent development of live imaging systems for various stages of mouse development and for different tissues [26–32] raised an interest in fluorescent reporters that quantitatively reflect the endogenous expression of lineage-specific genes.

In this study, we have carried out an *in vivo* fluorescence gene-trap screen, to our knowledge for the first time in the mouse embryo, using lentiviral transgenesis and generated reporter mice that express Venus specifically in one of the first lineages to be established during mammalian development. These newly established resources, when combined with live imaging microscopy, allowed us to directly connect gene expression dynamics with morphogenetic cellular processes. Taking advantage of this, we present a pipeline to integrate quantitative four-dimensional image analysis into an enhanced lineage map, which allowed us to identify lineage-specific gene regulation. This will lay the foundation for an integrative analysis of mouse embryonic development.

Results

Gene-trap screen generated fluorescence reporter mice for lineage-specific gene expression

We wished to establish an experimental system for monitoring expression dynamics of lineage-specific genes during early mouse embryogenesis. In order to acquire transgenic mice expressing a fluorescent gene expression reporter that allows quantitative expression analysis integrating morphogenetic information, we carried out a fluorescence gene-trap screen in the early mouse embryo using lentiviral transgenesis. One of the goals of this pilot study was to generate fluorescence reporter mice for each of the cell lineages in the blastocyst, specifically TE and ICM that includes epiblast and primitive endoderm.

A lentiviral gene-trap vector was designed with a promoter-less Venus reporter (thus the screen was named as Venus trap) so that upon integration into the transcribed region of an active gene, Venus would be expressed under the control of the promoter and enhancers of this gene (Fig 1A). Furthermore, Venus is tagged with a nuclear localization signal (NLS) to concentrate the fluorescent signal. To achieve efficient viral transduction while minimizing the degree of mosaicism, we transduced 2-cell stage embryos with the resulting vector (see Materials and Methods for details).

The screen was performed in two steps (Fig 1B). First, expression of the Venus fluorescent reporter was examined in the blastocyst at embryonic day 4.5 (E4.5), that is, 3 days after lentiviral transduction. Blastocysts yielding a positive signal upon brief microscopic inspection (21.8%; $n = 462$ blastocysts of $n = 2,121$ transduced 2-cell embryos; Fig 1C) were then transferred to the uterus of the foster mothers. This resulted in the generation of a total of $n = 107$ founder mice (F0) named VET or fVET after Venus trap for male or female founders, respectively. In a second screen, blastocysts of F1 generation for VET, or of F2 generation for fVET, were screened for fluorescence patterns. This screen identified 16 founder mice carrying at least one gene-trap integrant that, after germline transmission, express detectable levels of Venus in the blastocyst.

Southern blot analyses revealed that the 16 founder mice carry a total of 65 integrations with an average of 4.1 integrations per founder (Fig 1C and D). Integrations derived from one founder were labeled alphabetically in ascending order with "A" ascribed to the largest fragment. Integration sites, distributed over the entire chromosomes (Fig 1E), were cloned using ligation-mediated (LM)-PCR or TAIL-PCR, and trapped transcripts were cloned by 5′RACE (Table EV1). Cloned sequences were annotated using UCSC BLAT and Ensembl [33,34]. When single-integrant VET lines were derived by breedings with wild-type (wt) mice over generations, 23 of 65 integrations (35.4%) turned out to express the Venus reporter at a detectable level in the blastocyst (Fig 1C; Table EV1).

To characterize the overall change in expression during preimplantation development, we imaged live embryos of each of the 23 transgene-expressing single-integrant lines at E1.5, 2.5, 3.5 and 4.5 (Fig 2A). The images revealed distinct patterns of Venus expression among the active traps, indicating that the trapped genes are under specific spatio-temporal control during embryonic development. Importantly, specific expression patterns were maintained over more than 10 generations. They can be classified as follows: (i) ubiquitous, with similar fluorescence levels in all lineages ($n = 15$), (ii) specific to TE ($n = 3$), (iii) specific to ICM ($n = 2$), (iv) restricted to TE and primitive endoderm (PrE; $n = 2$) or (v) overall heterogeneous, with reporter expression only in a subset of blastomeres but without specificity for any particular lineage ($n = 1$). Altogether, we were able to establish nine of 23 gene-trap mouse lines (39.1%) in which the Venus reporter is expressed in a lineage-specific manner at the blastocyst stage, for example, Tmem50b$^{Gt(Venus)fVET17B}$ (hereafter written as Tmem50b^{Gt}) specific to TE (Fig 2B; Appendix Fig S1A; Movie EV1) and 2610305D13Rik$^{Gt(Venus)VET53A}$ (hereafter written as 2610305D13Rik^{Gt}) specific to ICM (Fig 2C; Appendix Fig S1B; Movie EV2; see Fig EV1 and Materials and Methods for more information on the identity of the gene trapped in VET53A, and Fig EV2 for additional lines with non-ubiquitous expression patterns). Lineage-specific expression of two of the trapped genes (Tmem50b^{Gt} and 2610305D13Rik^{Gt}) was also confirmed by qRT–PCR (Appendix Fig S2). In four of those lines, reporter expression
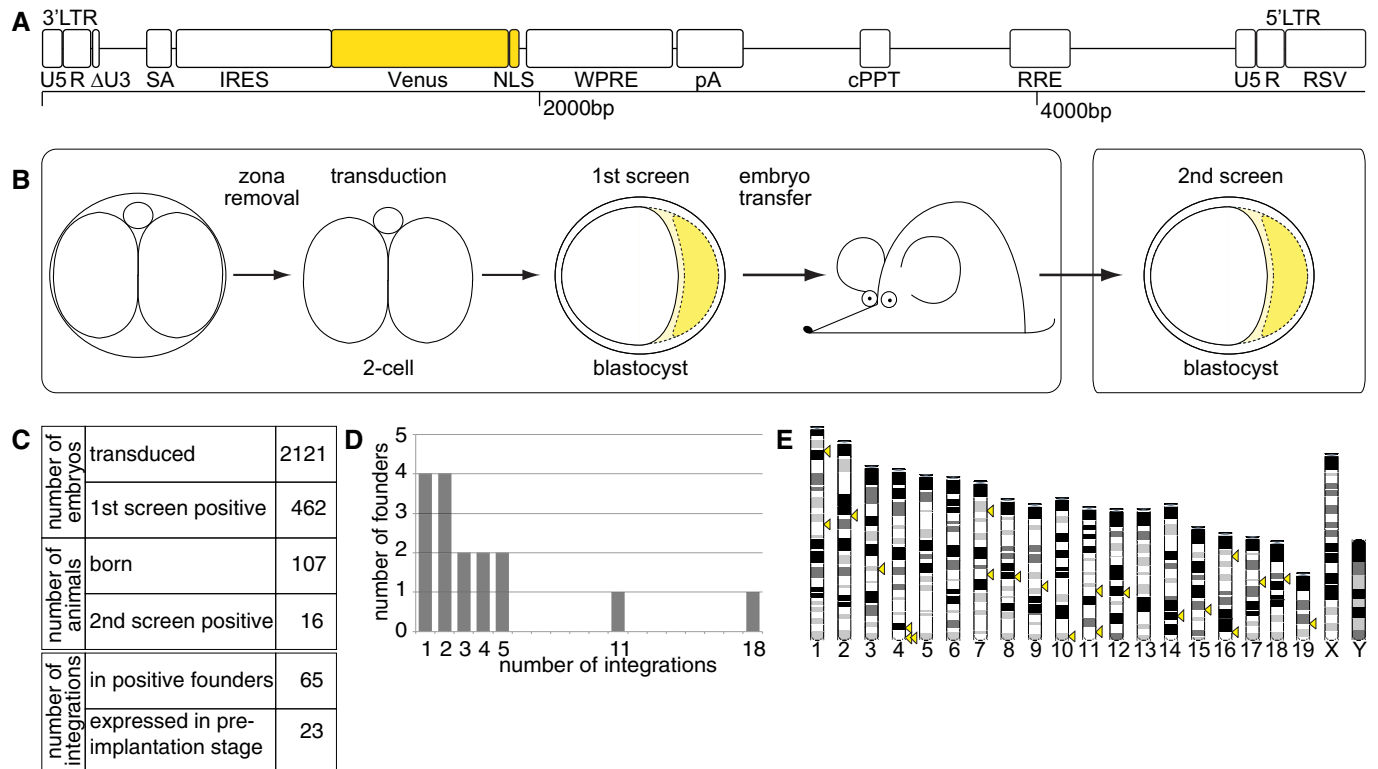
Figure 1. Design and outcome of the fluorescence gene-trap screen.

A Design of the fluorescence gene-trap vector. The gene-trap cassette consists of a splice acceptor (SA) followed by stop codons in all three reading frames and an internal ribosomal entry site (IRES). Venus is tagged with a nuclear localization signal (NLS). The essential virus-specific elements include self-inactivating long terminal repeat (LTR) consisting of U5, R and truncated U3 element (ΔU3); woodchuck hepatitis post-transcriptional regulatory element (WPRE); central poly-purine tract (cPPT); Rev-responsive element (RRE); and Rous sarcoma virus promoter (RSV).

B Design of the screenings. Denuded 2-cell stage embryos were transduced with the self-inactivating virus for 6–8 h. Blastocysts were first screened for fluorescence, indicating successful trapping of a gene after 3 days of *in vitro* culture. Positive embryos were then transferred to foster mothers to give rise to adult founders. Germline transmission of fluorescent signal-positive proviral integrants was tested in a fluorescence-based 2nd screen of expanded blastocysts of subsequent generations.

C Efficiency of the Venus-trap screen.

D Number of integrations identified in the founders positive in the 2nd screen.

E Distribution of integration sites among mouse chromosomes. Yellow triangles mark identified integration sites positive for Venus expression at the blastocyst stage (*n* = 22 of 23).

transiently exhibited a heterogeneous pattern before being confined to specific lineages (see the image of the E3.5 blastocyst for 2610305D13Rik[Gt] in Fig 2C, for Cd2ap[Gt] in Fig EV2B, for Rbfox2[Gt] in Fig EV2F and for Cers6[Gt] in Fig EV2G), with one exception (VET53C) having heterogeneous expression throughout the pre-implantation phase (see Fig EV2D).

Depending on the locus of genomic integration, a homozygous gene trap may result in a loss-of-function mutation [35,36]. This was observed with Ctnna1[Gt/Gt], for which the blastocyst cavity failed to expand (*n* = 15 embryos, *n* = 6 experiments; Fig EV3A1 and B1), a phenotype observed in an earlier gene-trap study [37]. We noted that fluorescent intensities are correlated with and could be used to determine the genotype of live VET embryos (Fig EV3A1 and A2, Kruskal–Wallis H-test, $P = 3 \times 10^{-5}$; Fig EV3A3 and A4, Kruskal–Wallis H-test, $P = 2 \times 10^{-6}$). Interestingly, Supt6[Gt/Gt] homozygotes died during pre-implantation development (*n* = 15 embryos, *n* = 4 independent experiments; Fig EV3A3 and B3). Loss of protein expression was confirmed by immunostaining (Fig EV3B1

and B2, Kruskal–Wallis H-test, $P = 10^{-5}$; Fig EV3B3 and B4, Kruskal–Wallis H-test, $P = 0.003$) and genotyping PCR of single embryos. These data demonstrate that VET insertions can produce functional KO by disrupting protein formation of the trapped gene. Furthermore, the Venus-trap screen allowed us to identify a new gene, *Supt6*, required for mouse pre-implantation development.

ICM and TE reporter expression is controlled under the lineage-specific genes

We examined the potential regulation of the newly identified lineage reporters through key factors of the emerging regulatory networks [38] by analyzing Venus expression of Tmem50b[Gt] or 2610305D13Rik[Gt] embryos in *Cdx2*^{−/−} or *Tead4*^{−/−} backgrounds. Tead4 and Cdx2 are required to maintain the TE lineage and its gene regulatory network [39–41]. Expression of the TE reporter Tmem50b[Gt] was reduced in a *Tead4*^{−/−} background (Fig 3A). Quantification
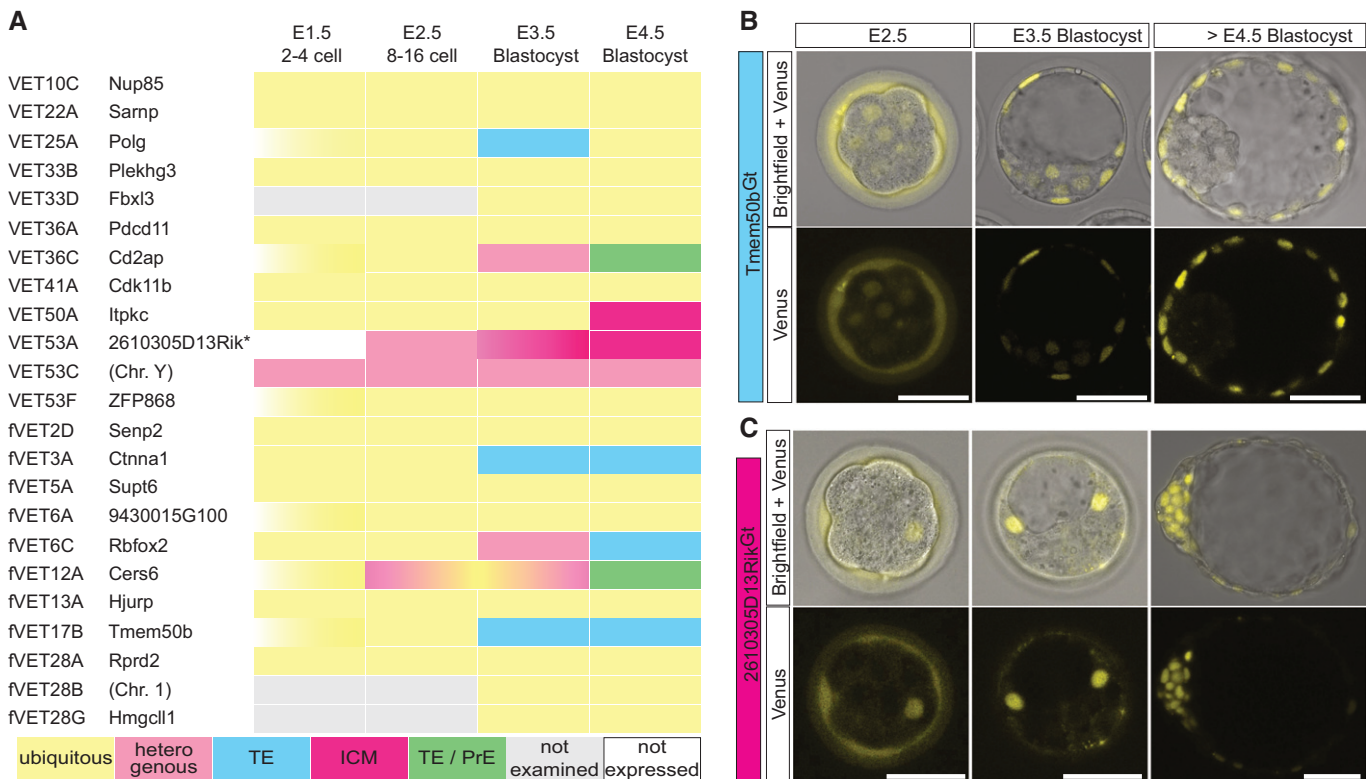
Figure 2. Spatio-temporal characterization of gene-trap mouse embryos.

A   The trapped gene and the Venus expression pattern of the established VET mouse lines, summarized as a result of $n \geq 3$ independent experiments for each line. *The trapped gene for VET53A is tentatively assigned as 2610305D13Rik (see Materials and Methods for details).

B, C   Brightfield and confocal live images of the developing embryos at E2.5 (8- to 16-cell stage morula), E3.5 and blastocyst cultured beyond E4.5 derived from the (B) TE-specific line Tmem50b^{Gt} and (C) ICM-specific line 2610305D13Rik^{Gt}. Scale bars are 50 μm. All fluorescent images are single confocal sections, representative for $n \geq 3$ independent experiments.

of the mean fluorescence intensity of the Tmem50b^{Gt} reporter in individual nuclei of outer cells of $Tead4^{+/+}$ ($n = 4$ embryos, $n = 16$ nuclei), $Tead4^{+/-}$ ($n = 4$ embryos, $n = 16$ nuclei) and $Tead4^{-/-}$ embryos ($n = 5$ embryos, $n = 19$ nuclei) revealed that the TE reporter Tmem50b^{Gt} is positively regulated by Tead4 (Fig 3B; Kruskal–Wallis H-test, $P = 10^{-8}$). Similarly, quantification of the Tmem50b^{Gt} mean fluorescence intensity in individual nuclei of outer cells of $Cdx2^{+/+}$ ($n = 2$ embryos, $n = 9$ nuclei), $Cdx2^{+/-}$ ($n = 2$ embryos, $n = 10$ nuclei) and $Cdx2^{-/-}$ embryos ($n = 4$ embryos, $n = 22$ nuclei) revealed a positive regulation of Tmem50b^{Gt} by Cdx2 (Fig 3C and D; Kruskal–Wallis H-test, $P = 2 \times 10^{-6}$). In contrast, the ICM marker 2610305D13Rik^{Gt} was negatively regulated by Tead4 and Cdx2 as measured in individual nuclei of outer cells in $Tead4^{+/+}$ ($n = 3$ embryos, $n = 17$ nuclei), $Tead4^{+/-}$ ($n = 4$ embryos, $n = 15$ nuclei) and $Tead4^{-/-}$ embryos ($n = 5$ embryos, $n = 16$ nuclei) (Fig 3E and F; Kruskal–Wallis H-test, $P = 5 \times 10^{-5}$); and in $Cdx2^{+/+}$ ($n = 4$ embryos, $n = 15$ nuclei), $Cdx2^{+/-}$ ($n = 4$ embryos, $n = 16$ nuclei) and $Cdx2^{-/-}$ embryos ($n = 4$ embryos, $n = 14$ nuclei, Fig 3G and H; Kruskal–Wallis H-test, $P = 0.01$).

Altogether, these data place the newly identified genes, Tmem50b and 2610305D13Rik, under the control of the gene regulatory network establishing the TE and ICM cell fates in the pre-implantation mouse embryo.

Establishment of the lineage segregation map of mouse pre-implantation development

To establish a map of lineage segregation between ICM and TE in association with gene expression dynamics, we time-lapse imaged one representative VET line for each lineage, Tmem50b^{Gt} for TE and 2610305D13Rik^{Gt} for ICM, and followed gene expression dynamics in embryos developing from the 4-cell to expanding blastocyst stage (64-cell). Under the established imaging condition, 98.1% of the live-imaged embryos ($n = 53/54$ embryos, $n = 6$ independent experiments) successfully developed to the expanded blastocyst stage, suggesting that the established lineage map would reflect the physiological situation *in vivo*.

Combining our gene-trap lines with a transgenic mouse line ubiquitously expressing histone H2B tagged with mCherry (R26-H2B-mCherry [42]), we normalized the Venus signal to the mCherry signal, thereby correcting for systematic error arising from nuclear position within the embryo. Furthermore, to rightly assign a given cell position and fate [32], we used mTmG to obtain membrane signal (hereafter written as mT in this study [43]). A cell is defined as outside or TE if some part of the cell membrane is exposed to the outside, whereas inside or ICM cells are entirely surrounded by cell–cell contacts [4]. Cell membrane signal also helped identifying individual nuclei when the distance between them becomes small.
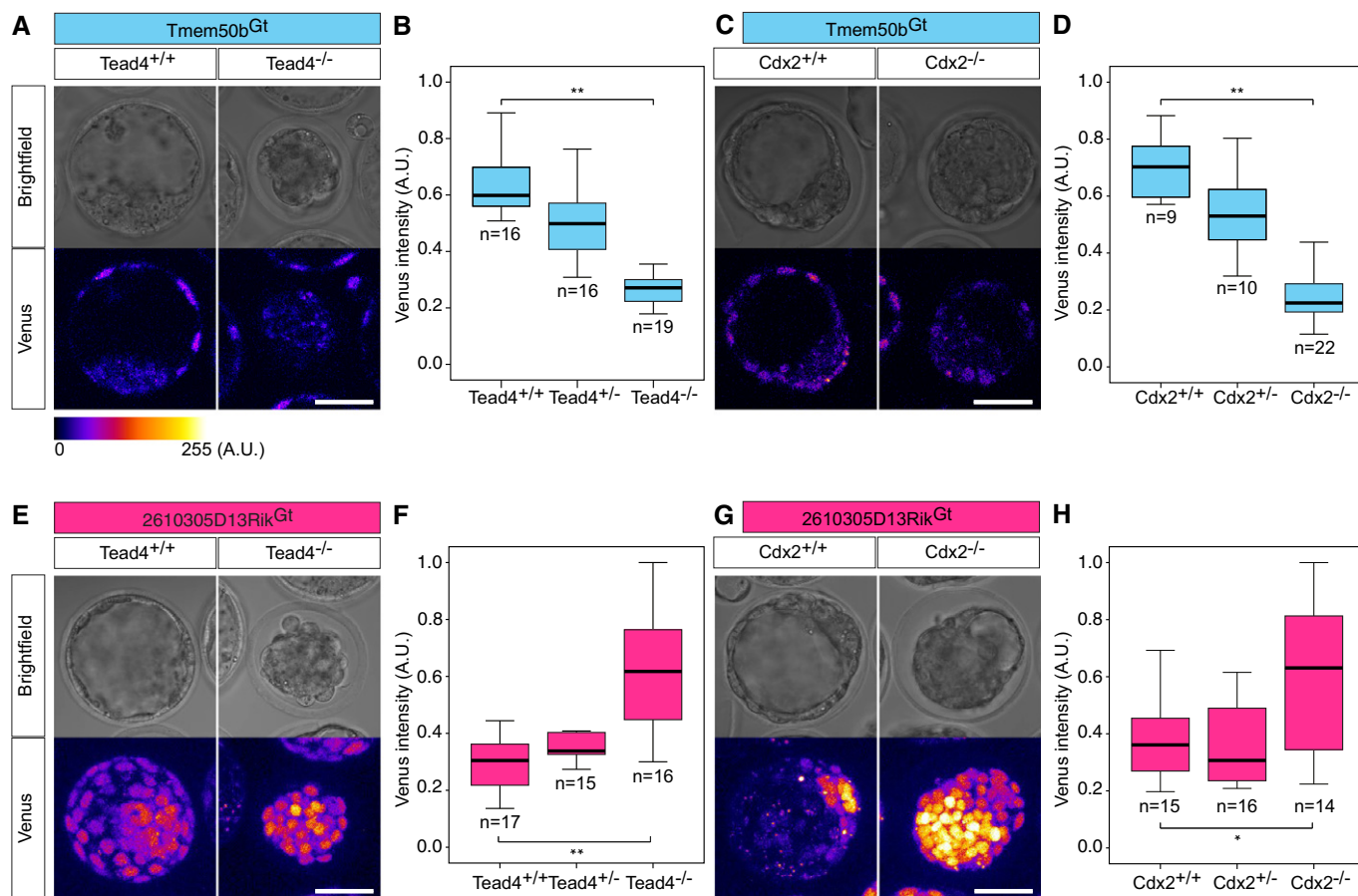
Figure 3. ICM and TE reporter expressions are controlled under the emerging lineage-specific genes.

A   Brightfield and confocal live images of Venus expression in Tmem50b^{Gt} in *Tead4$^{+/+}$* or *Tead4$^{-/-}$* background at E3.5 (*n* = 109 embryos in *n* = 3 experiments).

B   Box plots depicting Tmem50b^{Gt} Venus fluorescence intensities in individual nuclei of *Tead4$^{+/+}$* (*n* = 16 nuclei from *n* = 4 embryos), *Tead4$^{+/-}$* (*n* = 16 nuclei from *n* = 4 embryos) or *Tead4$^{-/-}$* embryos (*n* = 19 nuclei from *n* = 5 embryos; Kruskal–Wallis H-test, *P* = 10^{-8}).

C   Brightfield and confocal live images of Venus expression in individual nuclei of Tmem50b^{Gt} in a *Cdx2$^{+/+}$* or *Cdx2$^{-/-}$* background at E3.5 (*n* = 57 embryos in *n* = 5 experiments).

D   Box plots depicting Tmem50b^{Gt} Venus intensities in individual nuclei of *Cdx2$^{+/+}$* (*n* = 9 nuclei from *n* = 2 embryos), *Cdx2$^{+/-}$* (*n* = 10 nuclei from *n* = 2 embryos) or *Cdx2$^{-/-}$* embryos (*n* = 22 nuclei from *n* = 4 embryos; Kruskal–Wallis H-test, *P* = 2×10^{-6}).

E   Brightfield and confocal live images of Venus expression in 2610305D13Rik^{Gt} in a *Tead4$^{+/+}$* or *Tead4$^{-/-}$* background at E3.5 (*n* = 68 embryos in *n* = 3 experiments).

F   Box plots depicting 2610305D13Rik^{Gt} Venus intensities in individual nuclei of TE cells in *Tead4$^{+/+}$* (*n* = 17 nuclei from *n* = 3 embryos), *Tead4$^{+/-}$* (*n* = 15 nuclei from *n* = 4 embryos) or *Tead4$^{-/-}$* embryos (*n* = 16 nuclei from *n* = 5 embryos; Kruskal–Wallis H-test, *P* = 5×10^{-5}).

G   Brightfield and confocal live images of Venus expression in 2610305D13Rik^{Gt} in a *Cdx2$^{+/+}$* or *Cdx2$^{-/-}$* background at E3.5 (*n* = 95 embryos in *n* = 4 experiments).

H   Box plots depicting 2610305D13Rik^{Gt} Venus intensities in individual nuclei of TE cells in *Cdx2$^{+/+}$* (*n* = 15 nuclei from *n* = 4 embryos), *Cdx2$^{+/-}$* (*n* = 16 nuclei from *n* = 4 embryos) or *Cdx2$^{-/-}$* embryos (*n* = 14 nuclei from *n* = 4 embryos; Kruskal–Wallis H-test, *P* = 0.01).

Data information: Venus intensities in (B, D, F, H) are normalized to the highest level of expression. Statistical significance is indicated as * (*P* < 0.05) or ** (*P* < 0.001). Scale bars are 50 μm. Venus expression images are sum intensity projections with a fire LUT. A fire LUT from 0 to 255 gray scales is shown in (A).

Altogether, we prepared a triple transgenic embryo for quantitative gene expression analysis: a VET line combined with R26-H2B-mCherry and mT.

A representative image of the Tmem50b^{Gt}-Venus x R26-H2B-mCherry x mT embryo developing from the 8- to 64-cell stage is shown in Fig 4A. The Tmem50b^{Gt} reporter expression became detectable at 8- to 16-cell stage in all blastomeres. Subsequently, expression was specifically upregulated in the outside cells at around the E3.5 (> 32-cell) stage and, ultimately in the E4.5 blasto-cyst (≥ 64-cell), was restricted to the outside TE cells (Fig 4A; Movie EV3). On the other hand, 2610305D13Rik^{Gt}-Venus × R26-H2B-mCherry × mT embryos exhibited heterogeneous Venus expression pattern from 8- to 16-cell until E3.5 blastocyst, irrespective of any specific position of the cell within the embryo (Fig 4B; Movie EV4). The ICM-specific expression became restricted only at late E4.5 (≥ 128-cell) blastocyst.

To quantitatively characterize the expression dynamics of the VET reporters for Tmem50b and 2610305D13Rik genes during blastocyst development, we segmented the nuclei, tracked their trajectories through divisions, measured the signal intensity for Venus and normalized it against that of H2B-mCherry. This allowed us to fully track and quantify the dynamic change in expression of Tmem50b^{Gt}
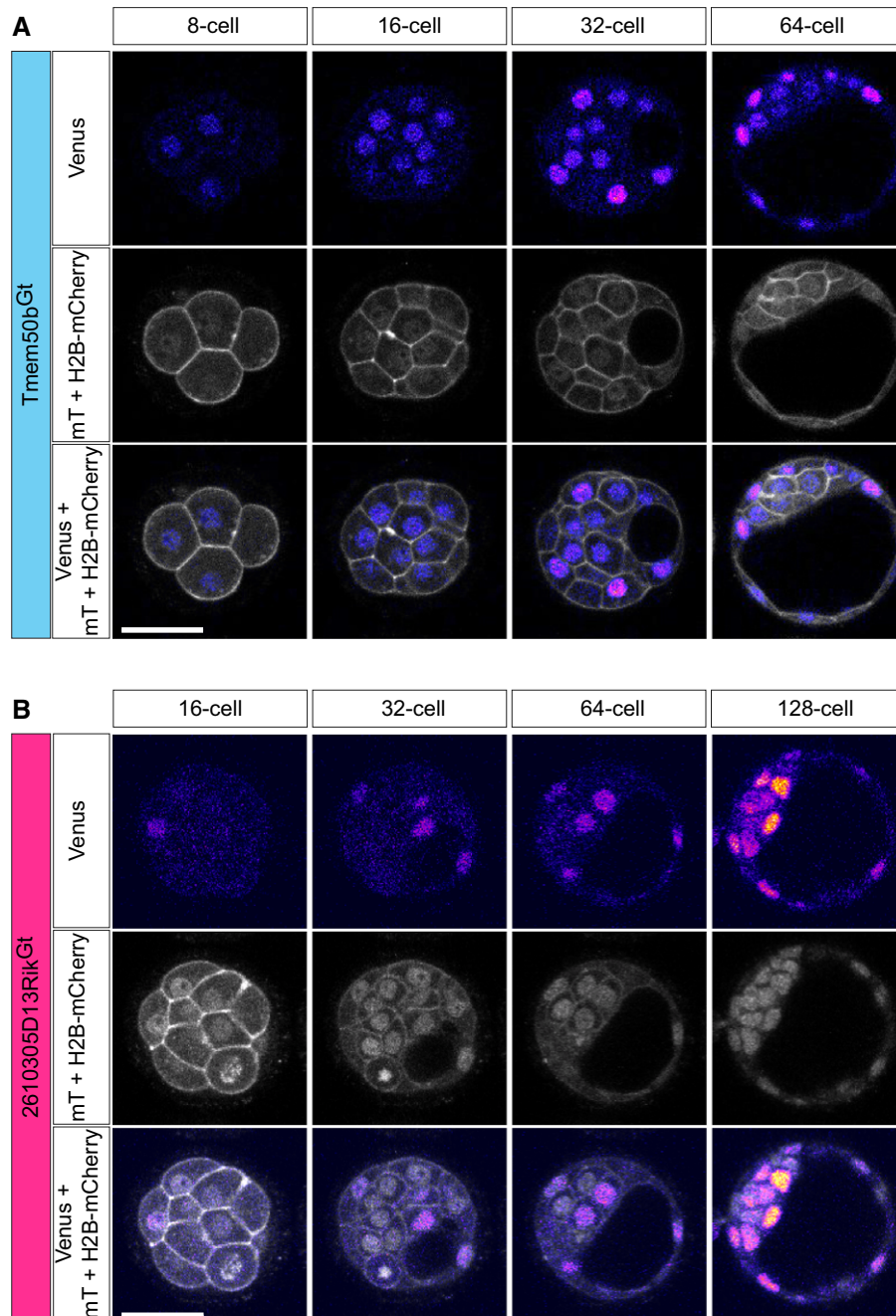
Figure 4.   Four-dimensional live imaging of the pre-implantation development of ICM and TE lineage reporter mice.

A   Representative images of a Tmem50b[Gt]-Venus × R26-H2B-mCherry × mT embryo developing from the 8- to 64-cell stage (n = 27 embryos in n = 3 experiments). Upper row panels show Venus expression, middle panels mT and H2B-mCherry expression, and lower panels all fluorescent channels merged.

B   Representative images of a 2610305D13Rik[Gt]-Venus × R26-H2B-mCherry × mT embryo developing from the 16- to 128-cell stage (n = 27 embryos in n = 3 experiments). Upper panels show Venus expression, middle panels mT and H2B-mCherry expression, and lower panels all fluorescent channels merged.

Data information: Scale bars are 50 μm. All images are single confocal sections and representative for $n \geq 3$ independent experiments. Venus expression images are shown using a fire LUT, and mT and mCherry are shown using a gray scale LUT.

(n = 3 embryos) and 2610305D13Rik[Gt] (n = 3 embryos) throughout 4 cell cycles over a 3-day period. A representative set of Venus expression data after tracking of all 8 blastomeres and its descendants in a single embryo is shown for Tmem50b[Gt] (Fig EV4A) and 2610305D13Rik[Gt] (Fig EV4B). Using the mT membrane signal, a

binary information on cell position was assigned at each time point as either "inside" (red line), when entirely surrounded by other cells, or "outside" (blue line), when part of the cell surface is exposed to the outside. In many cases, blastomeres did not stop in their position immediately after mitosis but progressively moved

toward their final position during interphase (see tracks changing from "blue" to "red" during interphase in Figs 5 and EV4; Appendix Figs S3 and S4), in agreement with recent live imaging studies [32,44–46].

Finally, all the extracted lineage relationships, gene expression dynamics and binary (inside or outside) cell-positional information were integrated into a comprehensive lineage map starting from the beginning of 8-cell until the late 32- or late 64-cell stage (Fig EV5). To supplement the binary cell-positional information, a relative position of nuclei along the embryonic radial axis was included in the map. The extracted nuclear position is effectively in agreement with the manually annotated binary cellular position. Altogether, we have established a complete lineage map of early mouse development in which lineage tracks are integrated with gene expression dynamics, absolute cell position and relative nuclei position (Fig 5, one representative map is shown for each lineage reporter, for which the expression dynamics are presented in Fig EV4; two more maps for each lineage are presented in
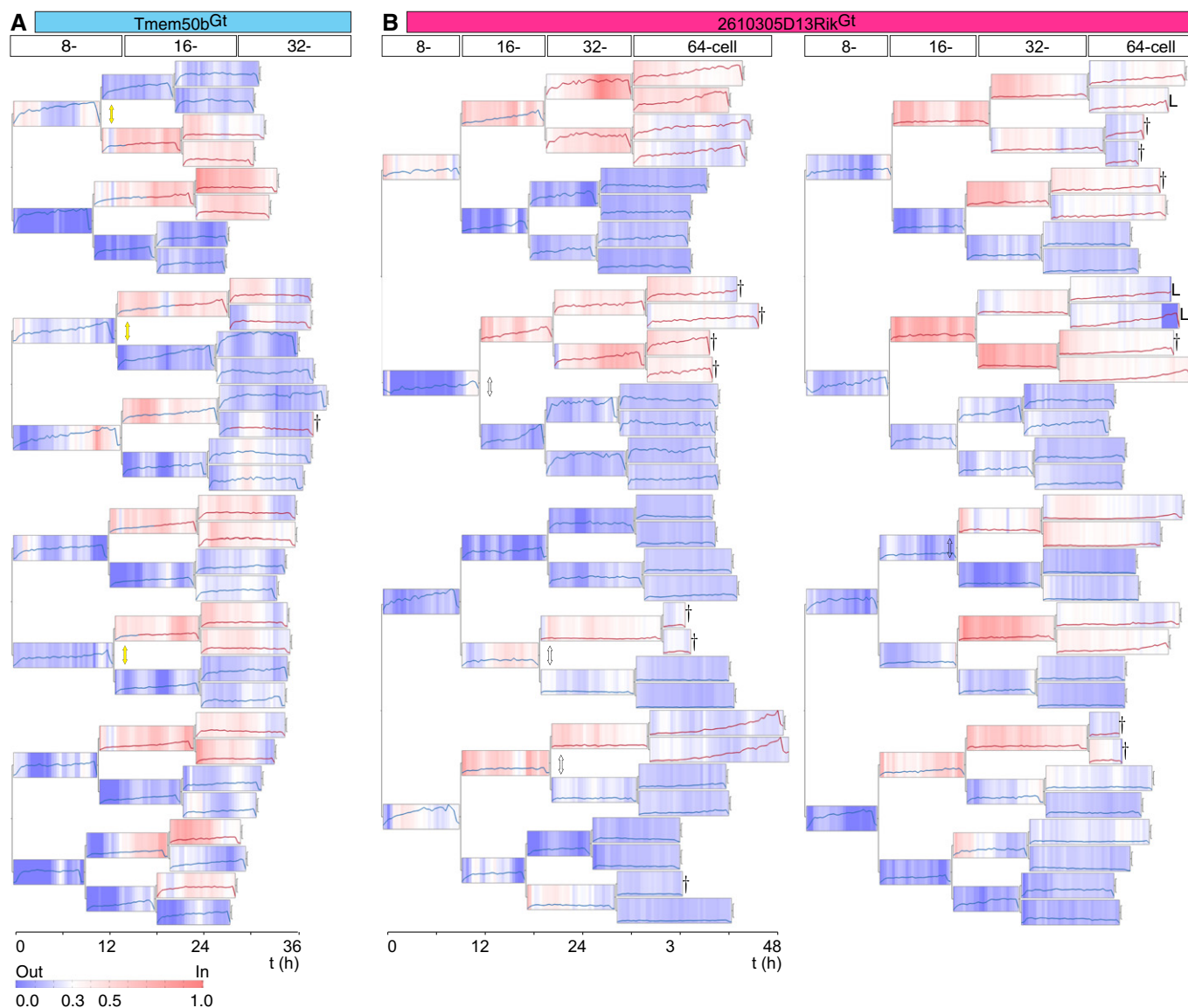

Figure 5. A lineage map of mouse pre-implantation development.

A, B   Lineage segregation maps of all cells of two embryos indicating cell position and a lineage reporter expression. (A) Lineages from the 8- to 32-cell stage based on live imaging a Tmem50b^{Gt}-Venus × R26-H2B-mCherry × mT embryo. Venus expression intensity is normalized first to mCherry and subsequently to the maximum expression intensity of all cells in the same cell cycle stage of an embryo. Each box in the lineage tree ranges from 0 to 1 in normalized expression. Blue and red lines indicate outside and inside cells, respectively. Blue–white–red scale indicates relative distance of nuclei to the surface of the embryo. Dagger marks cells undergoing apoptosis, and cell lineages lost during imaging are labeled with an "L". (B) Lineages from the 8- to 64-cell stage based on live imaging of a 2610305D13Rik^{Gt}-Venus × R26-H2B-mCherry × mT embryo. Arrows highlight representative descendant pairs as a result of asymmetric divisions (white: essentially no difference in the expression level; yellow: higher expression in the outside cell than in the inside cell).

Appendix Fig S3 for Tmem50b^{Gt} and in Appendix Fig S4 for 2610305D13Rik^{Gt}).

Quantitative expression analysis reveals distinct mechanisms underlying ICM and TE lineage specification

Using the established lineage maps, we wished to better understand the potential mechanism underlying ICM and TE lineage specification. For each lineage marker, we sought for the cue in the map that would allow us to predict the lineage, ICM or TE, at the earliest possible time in embryonic development.

First, we investigated the potential contribution of the division pattern to the regulation of lineage-specific gene expression. The orientation of the 8- to 16-cell division in relation to the cellular apico-basal axis was proposed to play a key role in the ICM vs. TE lineage segregation [2]. Indeed, we noted that many asymmetric divisions, defined in this study as a division generating one inside- and one outside-positioned descendant, are followed by an upregulation of Tmem50b^{Gt} in the outer descendant. Out of 48 divisions from 8- to 16-cell stage for all 6 embryos analyzed (3 each for Tmem50b^{Gt} and 2610305D13Rik^{Gt}), we identified 31 asymmetric divisions (64.6%), and out of 96 divisions from 16- to 32-cell stage, we identified 18 asymmetric divisions (18.8%). To examine the relationship between division pattern and gene expression, we have assembled the trajectories for all asymmetric divisions ($n = 16$ for 8- to 16-cell stage and $n = 7$ for 16- to 32-cell stage for Tmem50b^{Gt}, and $n = 15$ for 8- to 16-cell stage and $n = 11$ for 16- to 32-cell stage for 2610305D13Rik^{Gt}) and collectively compared the change in gene expression upon 8- to 16-cell and 16- to 32-cell divisions between the outer and inner descendants (Fig 6A–C). This sister cell analysis indicated that the Tmem50b^{Gt} expression is upregulated upon asymmetric division and becomes significantly higher in the outer cell as compared to the inner sister for both—8- to 16-cell and 16- to 32-cell—divisions (Fig 6A and C; $P = 0.0011$ and $P = 0.0019$ for 8- to 16- and 16- to 32-cell divisions, respectively, by two-sided Wilcoxon rank-sum test). In contrast, no such temporal change could be observed for 2610305D13Rik^{Gt} expression in the inside cells upon asymmetric division (Fig 6B and C; $P = 0.0158$ and $P = 0.0943$ for 8- to 16- and 16- to 32-cell divisions, respectively). The expression of 2610305D13Rik^{Gt} in outside cells becomes higher upon asymmetric 8- to 16-cell divisions; however, the overall level of expression remains low during 8- to 32-cell stages (see Fig EV4B), and the biological significance of this temporal change remains to be investigated. Taken together, these data suggest that asymmetric division drives the upregulation of a TE lineage marker expression specifically in the outer descendants, but it does not drive a reciprocal upregulation of an ICM lineage marker in the inner descendant.

Since the asymmetric 8- to 16-cell or 16- to 32-cell divisions did not upregulate the ICM reporter expression in the inside cells, we sought for other possible cues that would correlate with differential expression of the ICM reporter. From our VET reporter, the dynamics of gene expression could be more faithfully reflected in their increase than in their decrease, because dynamics of degradation of Venus-NLS protein may be different than those of the endogenous protein. As anticipated, live imaging of maternal Venus protein decay in wt embryos derived from a gene-trap line (Ctnna1$^{Gt/+}$) gave an estimate for the relevant half-life of 17 ± 3 h ($n = 16$, Appendix Fig S5). Thus, instead of the total level, we analyzed the average rate of the expression change for the Tmem50b^{Gt} reporter in outside and inside cells during 16- ($n = 32$ and $n = 16$) and 32-cell stages ($n = 56$ and $n = 40$), and for the 2610305D13Rik^{Gt} reporter in outside and inside cells during 16- ($n = 33$ and $n = 15$), 32- ($n = 53$ and $n = 41$) and 64-cell stages ($n = 106$ and $n = 84$; Fig 6D). As an alternative to the orientation of cell division, we investigated the possible role of cell position within the embryo (inside or outside) [1], in the regulation of lineage reporter expression. The data indicate that while the TE reporter Tmem50b^{Gt} is upregulated more strongly in outside cells than inside cells as early as at the 32-cell stage ($P = 2 \times 10^{-5}$), higher expression of the ICM reporter 2610305D13Rik^{Gt} in inside cells as compared to outside cells becomes evident only at the 64-cell stage ($P = 0.025$). Furthermore, in many cells that change position within the embryo from outside to inside, the expression of TE reporter remains low, whereas their sibling cells that remain outside upregulate the expression (Fig 5A, examples marked with yellow arrows). Therefore, cell position within the embryo indeed correlates with differential expression of our lineage reporters. Together, our lineage map allows us to faithfully allocate outer cell fate earlier than inner cell fate, in agreement with a recent study [32].

Discussion

In this study, we successfully generated novel lineage-specific fluorescent reporters by a fluorescence gene-trap screen in the mouse pre-implantation embryo. The screen was primarily designed to identify fluorescent reporter lines suitable for live imaging of pre-implantation development, while the possibility of examining the functional requirement of the trapped genes was subsidiary to the main goal. Generally, it would be ideal to generate a knock-in fluorescence-fusion reporter that would reflect the endogenous dynamics and function [18]. However, the successful use of such lines will crucially depend on the endogenous expression level of the gene and on the sensitivity of live imaging microscopy, precisely the signal detection efficiency relative to the laser illumination, since the mammalian embryo is particularly sensitive to light exposure [47]. In the present study, we adjusted the spatio-temporal resolution to enable manual tracking, positional annotation and segmentation of nuclei for signal quantitation while ensuring efficient development of the embryo. More advanced microscopy, for example, selective-plane illumination microscope (SPIM) [48,49], will allow live imaging of knock-in fluorescence-fusion reporters and with higher resolution for automated tracking and segmentation in the future. Using an unbiased approach, we aimed at discovering new markers for the first lineages in the early mouse embryo and fully characterized the expression dynamics of two genes with previously unknown specificity to ICM or TE lineage. This will be helpful to further study the gene network regulating lineage specification in the blastocyst.

We also present here advanced image analysis tools and strategies to include the increasing amount of information into lineage tracks to facilitate an integrative understanding of embryonic development and lineage segregation [16]. We developed a pipeline to establish a lineage map of embryonic development by live imaging the newly established VET lines and integrating gene expression dynamics and cell-positional information into lineage trees. These
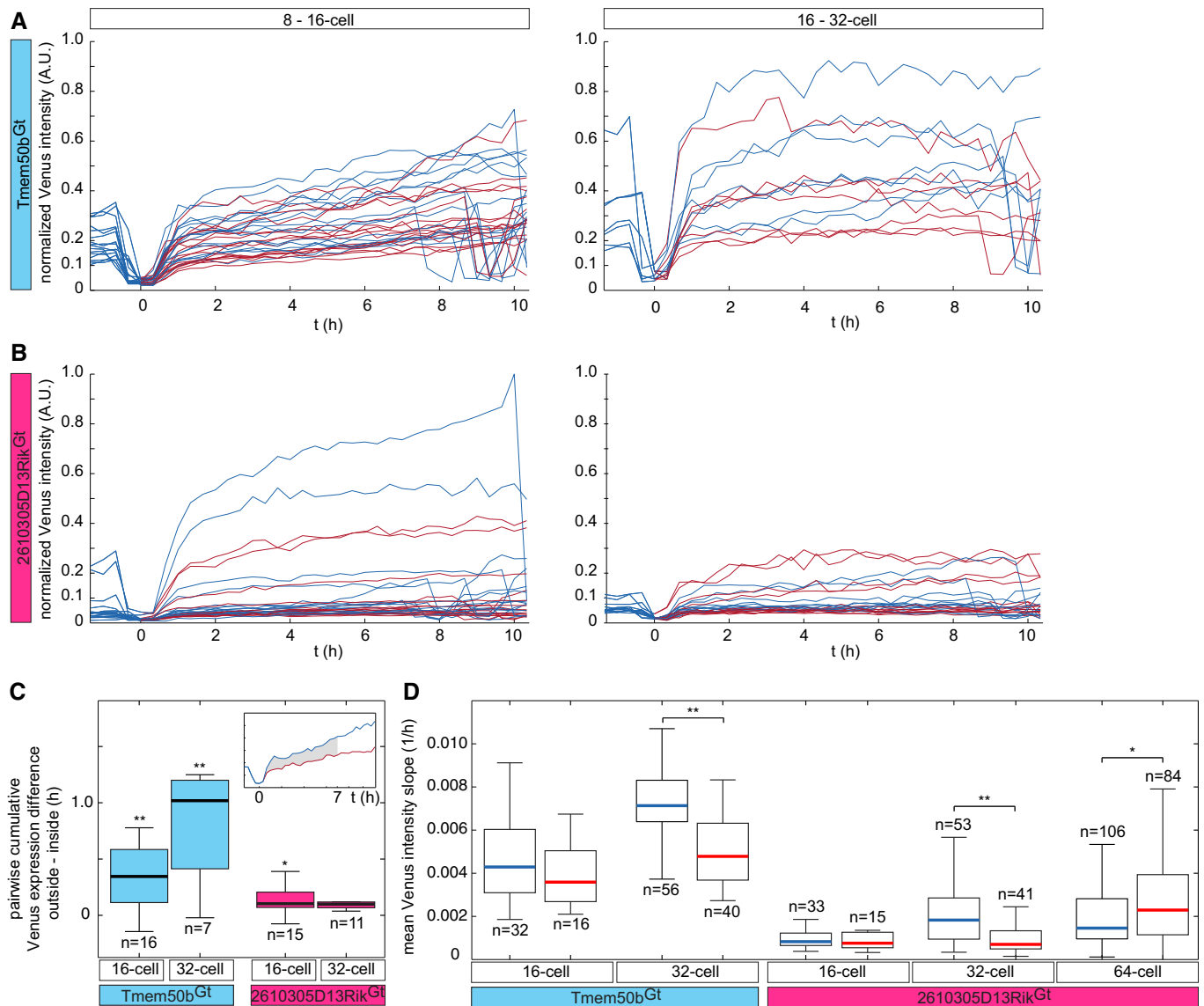
Figure 6. Quantitative analyses of the expression dynamics of TE and ICM lineage markers.

A Venus expression dynamics, normalized to mCherry signal, in cells of Tmem50b^{Gt}-Venus × R26-H2B-mCherry × mT embryos dividing asymmetrically from 8- to 16-cell (n = 16 divisions in n = 3 embryos) and 16- to 32-cell stage (n = 7 divisions in n = 3 embryos; see text and Materials and Methods for details). Blue and red lines indicate outside and inside cells, respectively. Time point of division is set at t = 0 h.

B Venus expression, normalized to mCherry signal, in cells of 2610305D13Rik^{Gt}-Venus × R26-H2B-mCherry × mT embryos dividing asymmetrically from 8- to 16-cell (n = 15 divisions in n = 3 embryos) and 16- to 32-cell stage (n = 11 divisions in n = 3 embryos).

C A pairwise difference of cumulative Venus expression between the descendants of asymmetric divisions (outside cell minus inside cell) at the 16- and 32-cell stages in Tmem50b^{Gt} (blue box plots; expression dynamics depicted in A; two-sided Wilcoxon rank-sum test; P (16-cell) = 0.0011; P (32-cell) = 0.0019) and 2610305D13Rik^{Gt} embryos (red box plots; depicted in B). Inset depicts an example taken from (A) in which the measured value is highlighted in gray.

D Mean rate of change of the normalized Venus intensity from t = 0 to 6 h after division in outside and inside cells for 16- (n = 32 and n = 16) and 32- (n = 56 and n = 40) cell stage in Tmem50b^{Gt} (left; Wilcoxon rank-sum test, P (32-cell) = $2 × 10^{-5}$) and for 16- (n = 33 and n = 15), 32- (n = 53 and n = 41) and 64- (n = 106 and n = 84) cell stages in 2610305D13Rik^{Gt} (right; Wilcoxon rank-sum test, P (64-cell) = 0.025) embryos. Blue and red median bars mark outside and inside cells, respectively. Statistical significance is indicated as * (P < 0.05) or ** (P < 0.001).

maps allowed us to analyze comprehensively and quantitatively gene expression dynamics as the first lineages are progressively segregated during mouse blastocyst development. Thus, our image analysis revealed gene expression dynamics in relation to particular morphogenetic processes. In light of the available models [1,2], we focused our analysis to the possible link between the cell division

pattern or cell position, and upregulation of lineage-specific gene expression. The systematic analyses presented here suggest that the expression of TE and ICM lineage markers is not initiated in a reciprocal and antagonistic manner as suggested earlier [2,3] but rather with different timings and through distinct mechanisms (Fig 7); namely, the upregulation of a TE lineage marker begins earlier and
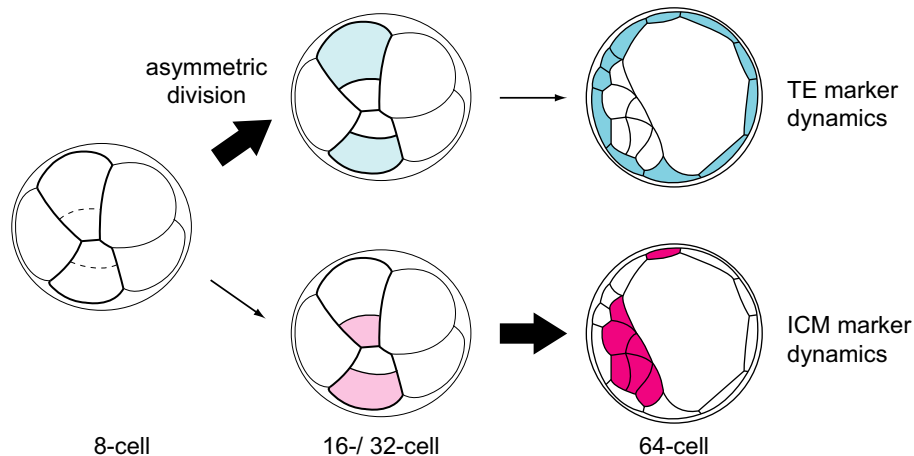
Figure 7. A new model for TE and ICM lineage segregation.
Distinct mechanisms for the acquisition of the TE or ICM molecular identity. TE or ICM molecular identity is acquired in a non-binary fashion and at different developmental times. The specific expression of a TE fate marker (blue) is established through asymmetric divisions from 8- to 16-cell and 16- to 32-cell stage, as quantified by our reporter mice. The ICM-specific gene (red) expression is non-reciprocal to the TE marker and only becomes ICM specific at the late 64-cell stage.

may be largely driven by asymmetric division, while that for the ICM marker may not be following the same mechanism. The mechanism regulating the ICM marker expression remains elusive, and the initiation of expression appears stochastic in the morula and early blastocyst stages without obvious correlation with position and the future lineage [4,8]. This finding is in line with our recent single-cell gene expression profiling study demonstrating genome-wide stochastic gene expression in the inner cells of the 32-cell stage blastocyst [7].

While in the current study image analysis was mostly performed manually, future development of automatic image processing will allow more comprehensive analysis with a large amount of image sets. This might help seeing through the apparently stochastic expression of the ICM markers. The fluorescent signals in a live embryo and its live imaging analysis will also allow to isolate a cell specifically expressing one, or eventually multiple, lineage marker(s) at a particular stage, and perform single-cell transcriptome analysis [7] to acquire comprehensive information of gene expression [16].

This study represents the first step in such an integrative approach, and its further development will enable us to understand the mechanisms underlying the early lineage segregation in the mammalian embryo.

Materials and Methods

Animal works, embryo recovery and culture

All animal works were performed in the animal facility at the Max Planck Institute for Molecular Biomedicine or at the European Molecular Biology Laboratory, according to the permission from the Landesamt für Natur, Umwelt und Verbraucherschutz NRW, Germany (projects #9.93.2.10.36.07.168 and #87-51.04.2010.A223) or to the permission by the institutional veterinarian overseeing the operation (ARC number TH11 00 11), respectively. The animal facilities are operating according to international animal welfare rules

(Federation for Laboratory Animal Science Associations guidelines and recommendations). No statistical method was used to estimate the sample size for animal experiments.

Isolation and culturing of embryos was performed as described previously [4]. Embryos were isolated from superovulated (C57BL/6xC3H) F1 female mice mated with (C57BL/6xC3H) F1 male mice. Superovulation was induced by intraperitoneal (ip) injection of 5 international units (IU) pregnant mare's serum gonadotropin (PMSG, Intervet Intergonan), followed by ip injection of 5 IU human chorionic gonadotropin (hCG, Intervet Ovogest 1500) 44–48 h later. Embryos were washed with FHM (Millipore, MR-024-D) several times and cultured in a 10 µl microdrop of KSOM (Millipore, MR-121-D) covered with mineral oil (Sigma, M8410 or Acros Organics) in 5% CO_2 atmosphere at 37°C.

Zygotes were recovered from oviduct ampullae 18–22 h after hCG injection. Cumulus cells were removed by briefly washing in 300 µg/ml hyaluronidase (Sigma, Typ IV-S, H4272) in FHM. Two-cell embryos to morulae were flushed from oviducts on day 1.5 to 2.5 after hCG injection with a fine canule (Acufirm, 1400 LL 23). Blastocysts were flushed from uteri on day 3.5 or 4.5 with a wide canule (Acufirm, 1400 LL 18). Embryos were handled using an aspirator tube (Sigma, A5177-5EA) or a hand pipette holder (Vitrolife, Sweden) equipped with a glass pipette pulled from Pasteur pipettes.

For the analysis shown in Fig 3, expression of Venus in *Cdx2* backgrounds was analyzed at E4.5. At E4.5, embryos reached the transition from 7th to 8th cell cycle (containing 65 to 128 cells to 129 to 256 cells). *Cdx2$^{+/+}$* embryos had 122.0 ± 23.3 cells ($n = 4$), *Cdx2$^{+/-}$* embryos had 136.0 ± 13.9 cells ($n = 4$), and *Cdx2$^{-/-}$* embryos had 118.5 ± 21.8 cells ($n = 4$) (average ± s.d.). Expression of Venus in *Tead4* embryos was analyzed at E3.5, because many cells of *Tead4$^{-/-}$* embryos began to show signs of apoptosis at E3.5 with fragmented chromosomes and could not be analyzed later. At E3.5, embryos reached the beginning of the 7th cell cycle (65 to 128 cells). *Tead4$^{+/+}$* embryos had $n = 72.2 \pm 7.8$ cells ($n = 5$), *Tead4$^{+/-}$* embryos had $n = 65.4 \pm 11.4$ cells ($n = 6$), and *Tead4$^{-/-}$* embryos had 66.7 ± 3.1 cells ($n = 6$) (average ± s.d.).

Lentiviral transgenesis

Delivery of the gene-trap cassette into the mouse genome was achieved using self-inactivating lentiviruses (sinLVs [50]). The pRRL-based lentiviral vector carries a gene-trap cassette with Venus as a fluorescent reporter (sinLV-pRRL-K; Fig 1A). To enhance the signal, Venus is coupled to the 39 nucleotides SV40-T-antigen nuclear localization signal (NLS) domain [51], followed by the woodchuck hepatitis post-transcriptional regulatory element (WPRE [52]) and the bovine growth hormone gene polyadenylation signal (pA [53]). The gene-trap cassette utilizes a 3′ splice consensus sequence from the type II adenovirus major late transcript intron 1/ exon 2 (splice acceptor, SA [54]) to trap 5′ splice consensus sequences (splice donors) from endogenous transcripts. Stop codons in all three reading frames prevent formation of a fusion protein, and the encephalomyocarditis virus (EMCV) internal ribosomal entry site (IRES [55]) guides translation of Venus-NLS. Additional elements non-essential for the gene-trap cassette are FRT sites [56] flanking the gene-trap cassette, as well as a LOXP2272 [57] and an AttB element [58] 5′ of the pA.

Lentiviruses were produced and harvested according to the published procedure [52] and were concentrated by ultracentrifugation to titers of 1 to 5.4×10^9 viral genomes per ml. Preliminary transduction of the mouse zygote using sinLV-pRRL-K was inefficient in producing embryos with detectable signal at the late blastocyst stage ($n = 1/54$ in three independent trials), whereas efficient transduction was achieved with the embryos infected at the 2-cell stage.

Two-cell embryos were prepared for transgenesis by removal of the zona pellucida through incubation in pronase (0.5% w/v Protease; Sigma, P8811) for 2–3 min. The denuded embryos were co-cultured with concentrated virus (2×10^8 to 1×10^9 HeLa-transducing units/ml) in FHM for 6–8 h. After three washes in FHM, the embryos were transferred to KSOM and cultured for 3 days. To prevent aggregation of embryos, individual denuded embryos were placed in microwells prepared with an aggregation needle (BLS) directly inside the microdrops of medium.

Identification of proviral integrations and the trapped genes

Genomic DNA was isolated from tail tissue, as described by The Jackson Laboratory (http://jaxmice.jax.org/support/genotyping/ tail_phenol.html), by digestion with proteinase K (Sigma, P2308, 0.5 mg/ml in 50 mM Tris–HCl (pH 8.0), 100 mM EDTA (pH 8.0), 100 mM NaCl, 1% SDS) at 55°C followed by purification with phenol–chloroform–isoamylalcohol (25:24:1, Roth, A156.1). The aqueous phase was separated from the organic phase using phase lock gels (5 Prime, VWR International, 713-2534). The gDNA was then precipitated with 100% ethanol (Roth, 9065.3), washed in 70% ice-cold ethanol and resuspended in 100 μl buffer TE (Invitrogen, 12090-015).

Proviral integration sites were detected by Southern blot. Southern blots were performed with a α-^{32}P-dCTP-labeled probe against Venus (711 bp *Nco*I/*Bsr*GI fragment). Ten micrograms of gDNA was digested with 250 U *Eco*RI (NEB, R0101M) for 12 h and subsequently loaded in 10 × 1 mm pockets on a 20 × 25 cm 0.8% agarose gel (Lonza). After 6–7 h at 120 V, the DNA in the gel was depurinated in 0.25 N HCl for 20 min and denatured in 0.5 M NaOH

and 1.5 M NaCl for two times 15 min, before blotting the DNA onto a nylon membrane (GE Healthcare, Nylon Hybond N, RPN203N). The membrane was neutralized in 0.05 M Na$_2$HPO$_4$·2H$_2$O at pH 6.5 for 30 min and then slightly dried between blotting papers (Schleicher & Schuell, GB005). The gDNA was then cross-linked to the membrane two times at 0.125 Joule. The cross-linked gDNA was pre-hybridized for 2 h at 65°C in pre-hybe buffer (5× SSC, 5× Denhardt's solution, 0.025 M NaH$_2$PO$_4$·H$_2$O at pH 6.5, 0.1% SDS, 0.1 mg/ml fish ssDNA in ddH$_2$O). This solution was then replaced with hybe buffer (pre-hybe buffer supplemented with 10% dextran sulfate Na salt) and α-^{32}P-dCTP-labeled Venus and incubated overnight. To radioactively label Venus, 75 ng DNA per 45 μl TE was processed with 2.5 μl α-^{32}P-dCTP (10 mCi/ml, Perkin-Elmer, Redivue) using the Rediprime II kit (GE Healthcare, RPN 1633) and purified using the ProbeQuant G-50 microcolumn (GE Healthcare, 28-9034-08) according to the manufacturer's protocol. Membranes were then washed two times for 15 min at room temperature in 2× SSC with 0.1% SDS and two times for 15 min at 65°C in 0.5× SSC with 0.1% SDS. Membranes were then exposed to calcium tungstate intensifying screens (Hyperscreen, GE Healthcare, RPN1663) at room temperature and analyzed on a phosphorimager (FLA-7000, Fujifilm). Additionally, membranes were exposed to films (Amersham Hyperfilm ECL, GE Healthcare, 28906837) at −80°C and developed (Agfa Curix 60).

Proviral integration sites were identified by ligation-mediated (LM)-PCR (modified from [59]). One microgram genomic DNA was *Mse*I (60 U, NEB R0525L)-digested and purified (Promega Wizard SV A 2360). Mse-linker oligos (Mse linker+: 5′-GTAATACGA CTCACTATAGGGCTCCGCTTAAGGGAC-3′, Mse linker−: 5′-PO$_4$-TAGTCCCTTAAGCGGAG-NH$_4$ (C7)-3′, 20 μM each) were hybridized by heating to 90°C and then decreasing the temperature to 1°C every 3 min to a final temperature of 20°C. In a total reaction volume of 20 μl, 3.5 μl of 20 μM MseI linker was ligated with 400 U T4 ligase (NEB, M0202S) to 13.5 μl *Mse*I-digested gDNA. To remove bacterial contamination and intra-proviral fragments, the ligation was digested with 40 U *Dpn*I (NEB, R0176) and 40 U *Sac*I (R0156) in 50 μl total volume for 4 h. A first PCR was performed in 25 μl total reaction volume using 5 μl processed gDNA, 0.3 μM of primers MKL-3 (5′-CTTAAGCCTCAATAAAGCTTGCCTTGAG-3′) and MseL1 (5′-GTAATACGACTCACTATAGGGC-3′) each, 0.2 mM dNTP mix, 0.5 μl *Taq* polymerase (Advantage 2, TaKaRa 639207) and 1× buffer. The thermal cycler settings were 1 min at 94°C (hot start), seven rounds of 2 s at 94°C and 1 min at 72°C, followed by 37 rounds of 2 s at 94°C and 1 min at 67°C and a final elongation step of 4 min at 72°C. Nested PCR was performed on 1 μl of a 1:200 dilution of the first PCR, 0.3 μM of primers MseL2 (5′-AGGGCTCCGCTTAAGGGAC-3′) and MKL-5 (5′-TGACTCTGG TAACTAGAGATCCCTCAG-3′) each, 0.2 mM dNTP mix, 0.5 μl *Taq* polymerase (Advantage 2) and 1× buffer. The thermal cycler settings for the nested PCR were 1 min at 94°C (hot start), five rounds of 2 s at 94°C and 1 min at 75°C, followed by 20 rounds of 2 s at 94°C and 1 min at 72°C and a final elongation step of 4 min at 72°C. The nested PCR product was run on a 0.8% agarose gel and purified (Qiagen, 28706). The isolated fragment was TOPO-TA cloned into pCR4 and transformed into TOP-Ten or DH5α *E. coli* and the bacteria plated according to the manufacturer's instructions (Invitrogen, TOPO-TA, K4575J10). Colonies were picked the following day and grown in LB medium with 50 μg/ml ampicillin

overnight at 37°C. Plasmids were purified using the QIAprep Spin system (Qiagen, 27106) and subsequently sequenced using M13 reverse primer.

Alternatively, integration sites were identified using thermal asymmetric interlaced (TAIL)-PCR [60,61] performed as described by [62], using the arbitrary degenerate primers and cycling conditions proposed there. Gene-specific primers were designed to identify either the region adjacent to the 3′-end of the integration (ISP-provirK-31 (5′-CTTTCCCCCTGGCCTTAACCGAATTT-3′), ISP-provirK-32 (5′-TTTTCCCATCGCGATCTAATTCTCCC-3′), ISP-provirK-33 (5′-GCTTAATACTGACGCTCTCGCACCCA-3′)) or the region adjacent to the 5′-end of the integration (ISP-provirK-51 (5′-GGGG ATCAATTCGAGCTCGGTACGA-3′), ISP-provirK-52 (5′-GGAACTT CACCGGTATTTGGGGGATC-3′), ISP-provirK-53 (5′-GGGATCAATT CGAGCTCGGTACCTTT-3′)).

The primary PCR was conducted using 3 μl gDNA in a total reaction volume of 20 μl (1× buffer, 1.5 mM MgCl$_2$, 0.2 mM dNTP (each), 0.15 μM ISP 1.3 μM AD primer, 1 U *Taq* DNA polymerase). Two microliters of a 1:20 dilution of this PCR was used as template in the secondary PCR with a total volume of 20 μl (1× buffer, 1.5 mM MgCl$_2$, 0.2 mM dNTP (each), 0.2 μM ISP 2, 2 μM AD primer, 1 U *Taq* DNA polymerase). Of this secondary PCR, 10 μl of a 1:10 dilution was used as template in the tertiary PCR with a total volume of 100 μl (1× buffer, 1.5 mM MgCl$_2$, 0.2 mM dNTP (each), 0.2 μM ISP 3.2 μM AD primer, 1 U *Taq* DNA polymerase). DNA fragments from tertiary reactions were purified, subcloned and amplified like DNA fragments from LM-PCR, using the pGEM®-T Easy Vector System (Promega, Fitchburg, USA) instead of the TOPO-TA system.

The cloned sequences were cleaned from vector, primer and proviral sequences to perform a BLAT search against genomic sequences of the GRCm38/mm10 (December 2011) or GRCm38.p3 (release 78; December 2014) assembly of the mouse (*Mus musculus*) genome (Fig EV1). In a few cases, it was difficult to unequivocally identify the integration site: The integration site for VET53A includes highly repetitive sequences that have an equally high homology to 2610305D13Rik, Rex2, Zfp600, Gm13145, Gm13242 and Gm13152. RT–PCRs, however, showed that only 2610305D13Rik exhibits the expression specific to ICM cells in E4.5 blastocysts but not in E3.5 blastocysts, in a manner consistent with the Venus expression pattern (Appendix Fig S2A); thus, the trapped gene was tentatively assigned as 2610305D13Rik (marked by an asterisk in Fig 2A). The integration site for VET53C is assigned as "X" (hidden) and the Venus signal was always detected in males, suggesting that the integration site is on Y chromosome for which the available sequence information is limited. The integration sites were mapped to karyotype ideograms (Fig 1E) using the Ensembl Karyoview. Trapped transcripts were detected by 5′RACE as described below and searched against cDNAs (transcripts/splice variants; BLASTN) or genomic sequences (BLAT) of the GRCm38.p3 (release 78; December 2014) assembly of the mouse genome (Fig EV1).

For genotyping VET mice, proviral integrants were detected by PCR on genomic DNA using a pair of primers specific for Venus (5′-TGAACCGCATCGAGCTGAAG-3′) and WPRE (5′-GCAA TGCCCCAACCAGT-3′) yielding a 671-bp fragment. Known integration sites were exponentially amplified by multiplex integration-site-specific PCR using a set of three primers, one inside the provirus

(5′-GGACTACTGCGCCCTACAGA-3′) and two specific for genomic sequences flanking the provirus. Specific primers are listed in Table EV1. Reactions were performed in a total volume of 20 μl containing 50 to 100 ng gDNA, 0.7× to 1.0× PCR buffer (+KCl/−MgCl$_2$), 1.5 mM to 2.5 mM MgCl$_2$, 0.2 mM dNTP mix (Fermentas, R0192), 0.4 μM of each primer and 0.5 U *Taq* polymerase (Fermentas, EP0402). The reaction was initiated at 94°C for 4 min, followed by 35 rounds of 1 min at 94°C, 1 min at 52°C to 62°C and 1 min at 72°C (see Table EV1 for details). An additional final elongation was performed for 7 min at 72°C.

5′ Rapid amplification of cDNA ends (RACE)

First-strand cDNA was synthesized from purified total RNA using 400 U reverse transcriptase (SuperScript III, Invitrogen, 18080), 5 mM DTT, 1× buffer, 2 pmol specific primer IRES-2 (5′-AACTCA-CAACGTGGCACTGG-3′), 30 U RNase inhibitor (Qiagen, 129918) and 0.5 mM dNTPs (Fermentas, R0192) in a total volume of 20 μl. RNA was then degraded using ribonuclease H (Fermentas, EN0201) and subsequently purified using the Qiaex II gel extraction kit (Qiagen, 20021) following the manufacturers' protocols. First-strand cDNA was tailed using 30 U TdT (Invitrogen, 10533-065) in 1× buffer and 0.2 mM dATP (Invitrogen, 10216-018) in a total volume of 20 μl. First PCR was performed on 2 μl tailed cDNA using primers QA (5′-CCAGTGAGCAGAGTGACGAGGAC-3′) and IRES-(−) (5′-CCTCACATTGCCAAAAGACGGC-3′) at 0.4 μM and QT (5′-CCAGT-GAGCAGAGTGACGAGGACTCGAGCTCAAGCTTTTTTTTTTTTTTTT T-3′) at 0.02 μM in the PCR master mix (Genaxxon, M3014) in a total volume of 50 μl. Second PCR was performed on 1 μl of a 1: 50 dilution of the first PCR product using primers QB (5′-GACGAG-GACTCGAGCTCAAGC-3′) and O-IRES-1b-(−) (5′-CAAACGCA CACCGGCCTTATTC-3′) at 0.4 μM and QT at 0.02 μM in the PCR Mastermix (Genaxxon, M0314). The second PCR product was purified from 1% agarose gel and TOPO-TA cloned before sequencing as described above.

Genotyping of single embryos

After live imaging Tmem50b^{Gt} or 2610305D13Rik^{Gt} embryos in *Tead4*$^{−/−}$ or *Cdx2*$^{−/−}$ backgrounds, embryo genotypes were assessed by genomic PCR of single embryos. Embryos were transferred to lysis buffer containing proteinase K (0.2 μg/μl) and 1× PCR buffer (with KCl, Fermentas, EP0402) in H$_2$O. Lysis was performed at 55°C for 1 h and 96°C for 10 min. For PCR, 2 to 5 μl of the lysate was used. Cdx2 < tm1Fbe > (MGI: 1857928) and Tead4 < IRES-lacZ > (RIKEN accession number: CDB0409K) embryos were genotyped as described elsewhere [41,63], whereas 2610305D13Rik^{Gt}, Tmem50b^{Gt}, Ctnna1^{Gt} and Supt6^{Gt} were genotyped as described above.

Total RNA isolation from placenta

For homogenization, placentas were washed in PBS, snap-frozen in the vapor phase of liquid nitrogen and after addition of 600 μl lysis buffer RLT (Qiagen, RNeasy Mini Kit, 74104) treated with a Precellys 24 using 1.4-mm ceramic beads at 5,000 rpm for 15 s. Total RNA was isolated using the RNeasy Mini Kit (Qiagen, 74104) using the manufacturer's protocol.

Isolation of trophectoderm cells by manual bisection of the blastocyst

TE cell samples were collected from E4.5 embryos after they hatched from the zona pellucida. E4.5–E4.75 blastocysts were manually bisected at the ICM-blastocyst cavity boundary by cutting with a 30Gx1/2 needle (BD, 305771) and removing polar TE cells and the ICM cells. The remaining mural TE cells were immediately transferred to 100 μl TRI reagent (Ambion, AM9738) at 4°C and stored at −20°C until RNA extraction.

RNA isolation from trophectoderm cells and reverse transcription

To extract RNA, 20% v/v of trichloromethane was added to TE samples in TRI reagent, followed by 15 min centrifugation at 4°C at 12,000 rpm. The supernatant was transferred into a fresh tube together with 50% v/v 2-propanol and 3 μl glycogen (Ambion, AM9510). Samples were incubated for 15 min on ice and centrifuged for 30 min at 4°C at 12,000 rpm, and the supernatant was discarded. The pellet was washed with 80% ethanol and dried. Reverse transcription was performed using SuperScript® III First-Strand Synthesis System for RT–PCR (Life Technologies, 18080-051) according to the manufacturer's instructions, using oligo $(dT)_{20}$ priming method. The cDNA synthesis was performed for 1 h.

qRT–PCR

Single-cell cDNA samples for qRT–PCR were prepared by Y. Onishi, and inside–outside position was determined as described in [7]. qRT–PCR was performed using SYBR® Green PCR Master Mix (Life Technologies, 4309155) on ABI StepOne devices (Life Technologies, 4376357, Ser. No. 272006386) according to the manufacturer's instruction with 5 μM primer concentration in 10 μl final sample volume, run for 40 cycles. Each sample was run in duplicates with a negative control and Gapdh as a housekeeping gene control, all in the same experiment. ES cell cDNA samples were added to each experiment in two dilutions to ensure normalized amplification between experiments. The primers sequences were as follows: Cdx2 (5′-ATTGTTTGCTGCTGTTCGAGTC-3′, 5′-CGACTTCCCTTCACCATA CAAC-3′), Gapdh (5′-ATGAATACGGCTACAGCAACAGG-3′, 5′-CTC TTGCTCAGTGTCCTTGCTG-3′), Gm13145 (5′-TGGACTTCTCATCGG AGGAA-3′, 5′-TGTTCCACGACCTTCTCCTT-3′), Gm13152 (5′-TAAT CCGGGCAACAAGAATG-3′, 5′-GCACAATGACCTCTGAGCAA-3′), Gm 13242 (5′-CTGCCAGATCAGAGGTCTCC-3′, 5′-TGGTGAGGAGCAAA CATTCA-3′), Oct4 (5′-GGCTCCTGATCAACAGCATCAC-3′, 5′-GATG CTGTGAGCCAAGGCAAG-3′), Rex2 (5′-TGCTCAGTCAACTCTCCGT AA-3′, 5′-TGGTGAGGAGCAAACATTCA-3′), Sox2 (5′-CATGAGAGC AAGTACTGGCAAG-3′, 5′-CCAACGATATCAACCTGCATGG-3′), Tm em50b (5′-GCGGTGGCTTCTCTATTCAT-3′, 5′-AAGAGAACCGTGTG CATTTT-3′), Zfp600 (5′-CATGGATGTGATGTTGGAGAA-3′, 5′-TGTG CTGTGTTTCTTGTTCCA-3′) and 2610305D13Rik (5′-TGAATGTTTG CTCCTCACCA-3′, 5′-TGAGACATTCCCATTCCTCTG-3′). Raw data were processed using StepOne Software (Life Technologies, version 2.3). A threshold for determining C_t values was set in the linear phase of amplification, at an equal value for the same gene in different experiments. The baseline was selected automatically and controlled manually for any software algorithm-induced mistakes.

After confirming sample and experiment quality by assessing negative control, ES cell cDNA amplification and melt curves, average values of the technical replicates were calculated for each gene. No replicates had to be excluded from the calculation. The ΔC_t value was calculated by subtracting the average C_t value of Gapdh from the average C_t value of the gene of interest for the same sample within the same experiment. Within a category (EPI, PE or TE cells), ΔC_t values for a single gene were used to calculate the average and standard deviation, as described in Appendix Fig S2. In negative controls and samples where cDNA for the gene in question was not present, the C_t value of one or both duplicates could not be determined by the StepOne Software algorithm. The average C_t value in such samples was set to the maximum experiment cycle number and used to calculate average and standard deviation for Appendix Fig S2A. Where melt curve analysis indicated a shift of the product melting temperature (T_m) to a different value (such as for 2610305D13Rik), the samples resulting from qRT–PCR reaction were additionally run on an agarose gel to identify the size of the product. The samples in which the product size did not correspond to that of control samples were marked by an asterisk in Appendix Fig S4, and the C_t values were not used to calculate average and standard deviation. For Appendix Fig S2B, ΔC_t value of samples marked with asterisk was set to a maximum value on the plot for representation purposes and does not reflect an actual ΔC_t as explained above. No statistical analysis of data distribution could be performed for samples in Appendix Fig S2 as no numerical value is available for several cells.

Immunohistochemistry

Embryos were fixed in 2% (for Supt6 and Ctnna1) or 4% (for other stainings) paraformaldehyde (Sigma, P6148) in PBS for 10 to 15 min. For stainings with anti-GFP antibody, the embryos were sorted into Venus positive and negative groups prior to fixation and remained separated throughout the procedure. After fixation, the embryos were washed with 0.1% Tween-20 (Sigma, P7949) in PBS (PBS-T) and permeabilized in 0.25% (for Supt6 and Ctnna1) or 0.5% (for other stainings) Triton X-100 (Sigma, T8787) in PBS for 30 min. Subsequently, the embryos were washed in PBS-T, blocked with 3% BSA in PBS-T (blocking solution) and incubated with the following primary antibodies in blocking solution at 4°C overnight: rabbit polyclonal anti-Spt6 (Abcam, ab32820, 1:2,000 dilution), rabbit monoclonal anti-Ctnna1 (Abcam, ab51032, 1:100 dilution), rabbit polyclonal anti-GFP (MBL, Code No. 598, 1:500 dilution) and goat polyclonal anti-Sox2 (Y-17, sc-17320, Santa Cruz Biotechnology, 1:100 dilution) or mouse monoclonal anti-Cdx2 (Biogenex, MU392-UC, 1:200 dilution). After washing in blocking solution, embryos were incubated with secondary antibodies as follows: for Supt6 and Ctnna1, 1 h with Alexa Fluor 546 donkey anti-rabbit (Life Technologies, A10040, 1:100 dilution) and Alexa Fluor 647 donkey anti-rabbit (Life Technologies, A31573, 1:100 dilution), respectively; for others, 2 h at room temperature with Alexa Fluor 488 donkey anti-goat (Life Technologies, A11055, 1:200 dilution) or Alexa Fluor 488 donkey anti-mouse (Life Technologies, A21202, 1:200 dilution) in addition to Alexa Flour 546 donkey anti-rabbit (Life Technologies, A10040, 1:200 dilution) and Phalloidin 633 (Life Technologies, A22284, 1:50 dilution), all in blocking solution. When nuclear

staining was required, the embryos were washed with PBS-T containing DAPI (Life Technologies, D3571, 1:2,000 dilution) and imaged immediately in the same solution. All incubation, washing and imaging steps were performed at room temperature unless stated otherwise. The stained embryos were imaged with LSM780 (Zeiss) equipped with a 40× water-immersion C-Apochromat 1.2 NA objective lens (Zeiss), using Zen 2010 software (Zeiss). The images were processed using Fiji running ImageJ (NIH, USA).

Live imaging microscopy

For microscopic analysis and live imaging, embryos were cultured in 5 µl drops prepared on a 0.17-mm glass-bottom dish (ZOG3, Elekon Science or MatTek, P35G-1.5-20C) in a 5% CO_2 chamber (PeCon). Temperature was maintained by a Tempcontrol 37–2 digital (Zeiss) at 37.5°C in a plastic chamber incubator XL (Zeiss) and a heatable mounting frame M-H (Zeiss), attached to a Zeiss Axiovert 200 M with Narishige manipulators. Fluorescence was detected with a Zeiss Axio Observer equipped with a 25×/0.8 LCI Plan Neofluar water-immersion objective lens (Zeiss). The light source was either a Colibri LED at 505 nm combined with a 60 HE filter set or a HXP lamp with a 46 HE filter set (Zeiss). For four-dimensional imaging, LSM780 (Zeiss) was used with a 40× water-immersion C-Apochromat 1.2 NA objective lens (Zeiss). Triple transgenic embryos carrying H2B-mCherry and membrane-tdTomato in addition to a Venus-trap reporter were prepared and imaged from 2- to 4-cell up to 128-cell stage (about 72 h). Venus was excited using a 514-nm argon laser, while mCherry and tdTomato were excited using a 561-nm DPSS laser. Z-stacks were recorded every 20 min and reconstructed from up to 55 images at 2 µm distance at 8-bit and 512 × 512 pixel resolution. Zen 2010 software (Zeiss) was used for the acquisition of images.

Half-life of the Venus-NLS protein was determined as decay of maternal Venus-NLS in wt embryos derived from mating heterozygous Ctnna1[Gt] mice (see Fig EV4). Four-cell stage blastomeres were dissociated in calcium- and magnesium-free KSOM medium (1/4-cell), as described previously [4] and imaged until 4/16-cell stage.

Image analysis

Image analysis was performed using AxioVision (Zeiss), Imaris (Bitplane), Fiji running ImageJ (USA) or Matlab (The MathWorks).

For lineage mapping (Figs 5 and EV4; Appendix Figs S3 and S4), a total of 364 cells were tracked until early 64-cell ($n = 3$ embryos for Tmem50b[Gt]) or late 64-cell ($n = 3$ embryos for 2610305D1 3Rik[Gt]; 94.8% of $n = 384$ cells). Due to blastocyst expansion, 14 cells were lost during tracking. A total of 54 cells (14.8%), in particular 47 of 83 ICM cells (56.6%) during the 64-cell stage, underwent nuclear DNA fragmentation, indicative of apoptosis [5].

Fluorescence signal in Figs 3 and EV3 was quantified using Fiji by manually selecting the area to be analyzed and extracting sum intensities from single confocal sections. Fluorescence intensities were normalized to the highest level of expression. Quantitation in Figs 5, 6 and EV4; Appendix Figs S3, S4 and S5 was done after four-dimensional lineage tracking. Segmentation was done manually or, if applicable, automatically using Imaris (Bitplane). Spots of 6 to 10 µm diameter were assigned to all nuclei based on Venus and/or H2B-mCherry signal. For Appendix Fig S4, Venus mean fluorescence intensities were normalized with the

highest level of expression. For Figs 5, 6 and EV4; Appendix Figs S3 and S4, Venus mean fluorescence intensities were normalized using nuclear mCherry mean fluorescence intensities. In the case of lineage maps shown in Fig 5; Appendix Figs S3 and S4, fluorescence intensity was further normalized to the maximum expression intensity of all cells in the same cell cycle stage of an embryo. In Figs 6 and EV4, the normalized Venus intensity was additionally normalized to the highest level of expression within the displayed set of data.

Binary information of cell position (inside or outside) was determined based on mT signal. Blastomeres with circumferential contacts to cells were defined to be inside, whereas blastomeres lacking circumferential contacts to cells were defined to be outside (see Fig EV5). Furthermore, relative position of nuclei was determined for each time point. For that, the approximate surface of the entire embryo was determined by finding the center of mass and the radius of a fitted hollow sphere, whose surface was closest to the convex hull of all nuclear positions. Nuclear positions were manually annotated using Imaris as described above. For each individual nucleus, the distance to the surface was calculated. Distant scales are defined in units of 1.2 times the radius of the calculated convex hull. Blue corresponds to nuclei close to the surface and red to nuclei deep inside the embryo. Nuclei outside the calculated convex hull with surface distances larger than 0.2 times radius were assigned the distance 0 (dark blue) as well. To generate lineage trees, spot-segmented nuclei were manually or, if applicable, automatically connected to tracks.

For the analysis shown in Fig 6A and B, the individual cell divisions of the same cell cycle stage were identified separately for all embryos carrying TE and ICM lineage markers. For each stage, the expression of the parent and the two descendant cells was plotted only if parent cells were found to be outside (blue) and one of the descendant cells was found to switch inside (red) within the following cell cycle stage. Time zero indicates the time point of division. The Venus expression intensity was normalized to the maximum intensity of all lineages within an embryo. In Fig 6C, for each pair of descendant blastomeres in Fig 6A and B, the difference in cumulative expression from 0 to 7 h post-division was measured for those tracks for which the expression data are available for the first 7 h (see inset in Fig 6C). For Fig 6D, Venus expression intensity was extracted as described for Fig 6A, except that expression curves of all descendant cells were included in the analysis. In this analysis, the curves rate of change was measured and averaged between 0 and 6 h for those tracks for which the expression data are available for the first 6 h.

Statistical analysis

Box plot graphs were generated, and statistical analyses were performed using IBM SPSS Statistics (version 22) and Matlab. No statistical methods were used to ensure adequate power to detect a pre-specified effect size. Samples were either chosen randomly for analysis without pre-established criteria or all available data were used. No randomization was applied and outcome assessment was not blinded.

For statistical analysis, data were first analyzed for normality using Shapiro–Wilk's test. Variance was either assessed using Levene's test or judged based on box plots. Non-parametric significance tests for

independent samples were performed for the analysis in Figs 3B, D, F and H, 6C and D, EV3A2, A4, B2 and B4, since many data sets were not normally distributed and variance was not always similar. For the analysis presented in Figs 3B, D, F and H and EV3A2, A4, B2 and B4, significance tests were performed pairwise using Kruskal–Wallis H-tests, because more than two groups were compared. For the analysis presented in Fig 6C and D, the two-sided Wilcoxon rank-sum test was performed. In Fig 6C, the sample distribution tested was derived by calculating a set of pairwise differences in cumulative Venus expression intensity of all descendant cells with all other descendant cells, effectively ignoring family relationships and inside–outside associations. The same test was performed pairwise in Fig 6D comparing inside and outside blastomeres.

Expanded View for this article is available online:
http://embor.embopress.org

Author contributions

J-ED and TH conceived and designed the study; J-ED performed the experiments presented in Figs 1–6 and EV1–5; Appendix Figs S3–S5 with the help of SW, AP and SS; and LP performed the experiments presented in Appendix Figs S1 and S2 with help of SS; SG, J-ED and LH performed image analyses presented in Figs 5, 6, EV4 and EV5; Appendix Figs S3 and S4. ACG and DT helped J-ED to generate lentiviral vectors and to analyze the integration sites. TH wrote the paper, except for Materials and Methods and Figure Legends written by J-ED and LP, with inputs from all authors.

Conflict of interest

The authors declare that they have no conflict of interest.

References

1. Tarkowski AK, Wróblewska J (1967) Development of blastomeres of mouse eggs isolated at the 4- and 8-cell stage. *J Embryol Exp Morphol* 18: 155–180

2. Johnson MH, Ziomek CA (1981) The foundation of two distinct cell lineages within the mouse morula. *Cell* 24: 71–80

3. Niwa H, Toyooka Y, Shimosato D, Strumpf D, Takahashi K, Yagi R, Rossant J (2005) Interaction between Oct3/4 and Cdx2 determines troph-ectoderm differentiation. *Cell* 123: 917–929

4. Dietrich J-E, Hiiragi T (2007) Stochastic patterning in the mouse pre-implantation embryo. *Development* 134: 4219–4231

5. Plusa B, Piliszek A, Frankenberg S, Artus J, Hadjantonakis A-K (2008) Distinct sequential cell behaviours direct primitive endoderm formation in the mouse blastocyst. *Development* 135: 3081–3091

6. Ralston A, Rossant J (2008) Cdx2 acts downstream of cell polarization to cell-autonomously promote trophectoderm fate in the early mouse embryo. *Dev Biol* 313: 614–629

7. Ohnishi Y, Huber W, Tsumura A, Kang M, Xenopoulos P, Kurimoto K, Oleś AK, Araúzo-Bravo MJ, Saitou M, Hadjantonakis A-K *et al* (2014) Cell-to-cell expression variability followed by signal reinforcement progressively segregates early mouse lineages. *Nat Cell Biol* 16: 280–281

8. Schrode N, Saiz N, Di Talia S, Hadjantonakis A-K (2014) GATA6 levels modulate primitive endoderm cell fate choice and timing in the mouse blastocyst. *Dev Cell* 29: 454–467

9. Hiiragi T, Solter D (2004) First cleavage plane of the mouse egg is not predetermined but defined by the topology of the two apposing pronuclei. *Nature* 430: 360–364

10. Srinivas S, Rodriguez T, Clements M, Smith JC, Beddington RSP (2004) Active cell migration drives the unilateral movements of the anterior visceral endoderm. *Development* 131: 1157–1164

11. Hadjantonakis A-K, Papaioannou VE (2004) Dynamic in vivo imaging and cell tracking using a histone fluorescent protein fusion in mice. *BMC Biotechnol* 4: 33

12. Motosugi N, Bauer T, Polanski Z, Solter D, Hiiragi T (2005) Polarity of the mouse embryo is established at blastocyst and is not prepatterned. *Genes Dev* 19: 1081–1092

13. Plusa B, Hadjantonakis A-K, Gray D, Piotrowska-Nitsche K, Jedrusik A, Papaioannou VE, Glover DM, Zernicka-Goetz M (2005) The first cleavage of the mouse zygote predicts the blastocyst axis. *Nature* 434: 391–395

14. Morris SA, Teo RTY, Li H, Robson P, Glover DM, Zernicka-Goetz M (2010) Origin and formation of the first two distinct cell types of the inner cell mass in the mouse embryo. *Proc Natl Acad Sci* 107: 6364–6369

15. Kurotaki Y, Hatta K, Nakao K, Nabeshima Y-I, Fujimori T (2007) [Supporting Online Material] Blastocyst axis is specified independently of early cell lineage but aligns with the ZP shape. *Science* 316: 719–723

16. Wennekamp S, Mesecke S, Nédélec F, Hiiragi T (2013) A self-organization framework for symmetry breaking in the mammalian embryo. *Nat Rev Mol Cell Biol* 14: 454–461

17. Hamilton TG, Klinghoffer RA, Corrin PD, Soriano P (2003) Evolutionary divergence of platelet-derived growth factor alpha receptor signaling mechanisms. *Mol Cell Biol* 23: 4013–4025

18. McDole K, Zheng Y (2012) Generation and live imaging of an endo-genous Cdx2 reporter mouse line. *Genesis* 50: 775–782

19. Xenopoulos P, Kang M, Puliafito A, Di Talia S, Hadjantonakis A-K (2015) Heterogeneities in Nanog expression drive stable commitment to pluri-potency in the mouse blastocyst. *Cell Rep* 10: 1508–1520

20. Filipczyk A, Gkatzis K, Fu J, Hoppe PS, Lickert H, Anastassiadis K, Schroeder T (2013) Biallelic expression of nanog protein in mouse embryonic stem cells. *Cell Stem Cell* 13: 12–13

21. Kawakami K, Takeda H, Kawakami N, Kobayashi M, Matsuda N, Mishina M (2004) A transposon-mediated gene trap approach identifies develop-mentally regulated genes in zebrafish. *Dev Cell* 7: 133–144

22. Larsen C, Franch-Marro X, Hartenstein V, Alexandre C, Vincent J-P (2006) An efficient promoter trap for detection of patterned gene expression and subsequent functional analysis in *Drosophila*. *Proc Natl Acad Sci USA* 103: 17813 – 17817

23. Morin X, Daneman R, Zavortink M, Chia W (2001) A protein trap strategy to detect GFP-tagged proteins expressed from their endogenous loci in *Drosophila*. *Proc Natl Acad Sci USA* 98: 15050 – 15055

24. International Mouse Knockout Consortium, Collins FS, Rossant J, Wurst W (2007) A mouse for all reasons. *Cell* 128: 9 – 13.

25. Stanford WL, Cohn JB, Cordes SP (2001) Gene-trap mutagenesis: past, present and beyond. *Nat Rev Genet* 2: 756 – 768

26. Kwon GS, Viotti M, Hadjantonakis A-K (2008) The endoderm of the mouse embryo arises by dynamic widespread intercalation of embryonic and extraembryonic lineages. *Dev Cell* 15: 509 – 520

27. Rompolas P, Deschene ER, Zito G, Gonzalez DG, Saotome I, Haberman AM, Greco V (2012) Live imaging of stem cell and progeny behaviour in physiological hair-follicle regeneration. *Nature* 487: 496 – 499

28. Snippert HJ, Flier LGVD, Sato T, Es JHV, Born MVD, Kroon-Veenboer C, Barker N, Klein AM, Rheenen JV, Simons BD *et al* (2010) Intestinal crypt homeostasis results from neutral competition between symmetrically dividing Lgr5 stem cells. *Cell* 143: 134 – 144

29. Srinivas S (2010) Imaging cell movements in egg-cylinder stage mouse embryos. *Cold Spring Harb Protoc* 2010: pdb.prot5539

30. Bedzhov I, Zernicka-Goetz M (2014) Self-organizing properties of mouse pluripotent cells initiate morphogenesis upon implantation. *Cell* 156: 1032 – 1044

31. Yamanaka Y, Tamplin OJ, Beckers A, Gossler A, Rossant J (2007) Live imaging and genetic analysis of mouse notochord formation reveals regional morphogenetic mechanisms. *Dev Cell* 13: 884 – 896

32. Watanabe T, Biggins JS, Tannan NB, Srinivas S (2014) Limited predictive value of blastomere angle of division in trophectoderm and inner cell mass specification. *Development* 141: 2279 – 2288

33. Hubbard T, Andrews D, Caccamo M, Cameron G, Chen Y, Clamp M, Clarke L, Coates G, Cox T, Cunningham F *et al* (2005) Ensembl 2005. *Nucleic Acids Res* 33: D447 – D453

34. Kent WJ, Sugnet CW, Furey TS, Roskin KM, Pringle TH, Zahler AM, Haussler D (2002) The human genome browser at UCSC. *Genome Res* 12: 996 – 1006

35. O'Kane CJ, Gehring WJ (1987) Detection in situ of genomic regulatory elements in *Drosophila*. *Proc Natl Acad Sci USA* 84: 9123 – 9127

36. Gossler A, Joyner AL, Rossant J, Skarnes WC (1989) Mouse embryonic stem cells and reporter constructs to detect developmentally regulated genes. *Science* 244: 463 – 465

37. Torres M, Stoykova A, Huber O, Chowdhury K, Bonaldo P, Mansouri A, Butz S, Kemler R, Gruss P (1997) An alpha-E-catenin gene trap mutation defines its function in preimplantation development. *Proc Natl Acad Sci USA* 94: 901 – 906

38. Sasaki H (2010) Mechanisms of trophectoderm fate specification in preimplantation mouse development. *Dev Growth Differ* 52: 263 – 273

39. Yagi R, Kohn MJ, Karavanova I, Kaneko KJ, Vullhorst D, DePamphilis ML, Buonanno A (2007) Transcription factor TEAD4 specifies the trophectoderm lineage at the beginning of mammalian development. *Development* 134: 3827 – 3836

40. Strumpf D, Mao C-A, Yamanaka Y, Ralston A, Chawengsaksophak K, Beck F, Rossant J (2005) Cdx2 is required for correct cell fate specification and differentiation of trophectoderm in the mouse blastocyst. *Development* 132: 2093 – 2102

41. Nishioka N, Yamamoto S, Kiyonari H, Sato H, Sawada A, Ota M, Nakao K, Sasaki H (2008) Tead4 is required for specification of trophectoderm in pre-implantation mouse embryos. *Mech Dev* 125: 270 – 283

42. Abe T, Kiyonari H, Shioi G, Inoue K-I, Nakao K, Aizawa S, Fujimori T (2011) Establishment of conditional reporter mouse lines at ROSA26 locus for live cell imaging. *Genesis* 49: 579 – 590

43. Muzumdar MD, Tasic B, Miyamichi K, Li L, Luo L (2007) A global double-fluorescent Cre reporter mouse. *Genesis* 45: 593 – 605

44. Anani S, Bhat S, Honma-Yamanaka N, Krawchuk D, Yamanaka Y (2014) Initiation of Hippo signaling is linked to polarity rather than to cell position in the pre-implantation mouse embryo. *Development* 141: 2813 – 2824

45. McDole K, Xiong Y, Iglesias PA, Zheng Y (2011) Lineage mapping the pre-implantation mouse embryo by two-photon microscopy, new insights into the segregation of cell fates. *Dev Biol* 355: 239 – 249

46. Yamanaka Y, Lanner F, Rossant J (2010) FGF signal-dependent segregation of primitive endoderm and epiblast in the mouse blastocyst. *Development* 137: 715 – 724

47. Takenaka M, Horiuchi T, Yanagimachi R (2007) Effects of light on development of mammalian zygotes. *Proc Natl Acad Sci USA* 104: 14289 – 14293

48. Krzic U, Gunther S, Saunders TE, Streichan SJ, Hufnagel L (2012) Multi-view light-sheet microscope for rapid in toto imaging. *Nat Meth* 9: 730 – 733

49. Tomer R, Khairy K, Amat F, Keller PJ (2012) Quantitative high-speed imaging of entire developing embryos with simultaneous multiview light-sheet microscopy. *Nat Meth* 9: 755 – 763

50. Dull T, Zufferey R, Kelly M, Mandel RJ, Nguyen M, Trono D, Naldini L (1998) A third-generation lentivirus vector with a conditional packaging system. *J Virol* 72: 8463 – 8471

51. Nagoshi E, Saini C, Bauer C, Laroche T, Naef F, Schibler U (2004) Circadian gene expression in individual fibroblasts: cell-autonomous and self-sustained oscillators pass time to daughter cells. *Cell* 119: 693 – 705

52. Zufferey R, Donello JE, Trono D, Hope TJ (1999) Woodchuck hepatitis virus posttranscriptional regulatory element enhances expression of transgenes delivered by retroviral vectors. *J Virol* 73: 2886 – 2892

53. Soriano P, Montgomery C, Geske R, Bradley A (1991) Targeted disruption of the c-src proto-oncogene leads to osteopetrosis in mice. *Cell* 64: 693 – 702

54. Friedrich G, Soriano P (1991) Promoter traps in embryonic stem cells: a genetic screen to identify and mutate developmental genes in mice. *Genes Dev* 5: 1513 – 1523

55. Jang SK, Kräusslich HG, Nicklin MJ, Duke GM, Palmenberg AC, Wimmer E (1988) A segment of the 5' nontranslated region of encephalomyocarditis virus RNA directs internal entry of ribosomes during in vitro translation. *J Virol* 62: 2636 – 2643

56. Andrews BJ, Proteau GA, Beatty LG, Sadowski PD (1985) The FLP recombinase of the 2 micron circle DNA of yeast: interaction with its target sequences. *Cell* 40: 795 – 803

57. Lee G, Saito I (1998) Role of nucleotide sequences of loxP spacer region in Cre-mediated recombination. *Gene* 216: 55 – 65

58. Landy A, Ross W (1977) Viral integration and excision: structure of the lambda att sites. *Science* 197: 1147 – 1160

59. Schröder ARW, Shinn P, Chen H, Berry C, Ecker JR, Bushman F (2002) HIV-1 integration in the human genome favors active genes and local hotspots. *Cell* 110: 521 – 529

60. Liu YG, Mitsukawa N, Oosumi T, Whittier RF (1995) Efficient isolation and mapping of *Arabidopsis thaliana* T-DNA insert junctions by thermal asymmetric interlaced PCR. *Plant J* 8: 457 – 463

61. Liu YG, Whittier RF (1995) Thermal asymmetric interlaced PCR: automatable amplification and sequencing of insert end fragments from P1 and YAC clones for chromosome walking. *Genomics* 25: 674 – 681

62. Pillai MM, Venkataraman GM, Kosak S, Torok-Storb B (2008) Integration site analysis in transgenic mice by thermal asymmetric interlaced (TAIL)-PCR: segregating multiple-integrant founder lines and determining zygosity. *Transgenic Res* 17: 749 – 754

63. Chawengsaksophak K, James R, Hammond VE, Köntgen F, Beck F (1997) Homeosis and intestinal tumours in Cdx2 mutant mice. *Nature* 386: 84 – 87